Progress in Quantum Electronics 86 (2022) 100438

Contents lists available at ScienceDirect

Progress in Quantum Electronics

journal homepage: www.elsevier.com/locate/pqe

Defect engineering of metal halide perovskite optoelectronic devices

Xuanyu Zhang [a], Xiongbin Wang [a,b], Huan Liu [a], Rui Chen [a,*]

[a] Department of Electrical and Electronic Engineering, Southern University of Science and Technology, Shenzhen, 518055, China
[b] Institute of Applied Physics and Materials Engineering, University of Macau, Avenida da Universidade, Taipa, Macau, 999078, China

ARTICLE INFO

Keywords:
Defects engineering
Metal halide perovskite
Solar cells
Light-emitting diodes

ABSTRACT

Recently, thanks to their unique and attractive properties, such as tunable bandgap, high absorption coefficient, and long charge carrier diffusion length, metal halide perovskites have been recognized as one of the emerging candidates for next-generation optoelectronic devices. Optoelectronic devices based on perovskites have achieved significant breakthroughs in a relatively short period of time. However, their commercialization still faces various challenges, including stability, scalability, and reproducibility. Defects are often the culprits behind these problems, either inside the perovskites or at the device interfaces. Therefore, rational utilization of defect engineering to minimize the effect of defects on device performance and control of carrier behavior is the key to achieve efficient and stable perovskite-based optoelectronic devices (PODs). Given the important contribution to the rapid development of PODs, there is an urgent need to systematically investigate and summarize recent research advances in defect engineering. Therefore, in this review, defect physics in PODs are described in detail, the role and importance of defects in various PODs are highlighted, and various strategies for optimizing PODs are reviewed. Finally, based on the latest progresses and breakthroughs, the challenges facing in the future development of metal halide perovskites and their potential significance in the field of the optoelectronic are prospected.

1. Introduction

Metal halide perovskites have received extensive research attention in recent years due to their excellent optoelectronic properties [1–5], which open applications in areas such as solar cells (SCs) [6–8], light-emitting diodes (LEDs) [9–11], field effect transistors (FETs) [12], and lasers [13], *etc*. Up to now, LEDs based on perovskite have achieved a maximum external quantum efficiency (EQE) of 23.4% [14], and the certified record power conversion efficiency (PCE) of perovskite SCs has reached 29.15% with a high fill factor (FF) up to 79.52% [15]. These perovskite-based optoelectronic devices (PODs) are already comparable to conventional devices such as silicon [16], GaAs [17], CIGS [18], and organic LEDs [19] fabricated via high-temperature vacuum processes.

The superior performance of PODs is directly derived from the unique crystal structure and chemical versatility of perovskite materials. As shown in Fig. 1a, metal halide perovskites have the general formula ABX_3, where A is a monovalent cation, usually inorganic cesium, organic methylammonium (MA, $CH_3NH_3^+$) or formamidinium (FA, $(NH_2)_2CH^+$), B is a divalent metal cation such as lead and tin, and X is halide anions. These ions play different roles in the perovskite lattice. For example, change the size of A cation can

* Corresponding author.
E-mail address: chenr@sustech.edu.cn (R. Chen).

https://doi.org/10.1016/j.pquantelec.2022.100438
Received 7 June 2022; Received in revised form 4 September 2022; Accepted 2 November 2022
Available online 8 November 2022

cause the expansion or contraction of the entire lattice, affecting the electronic properties [20,21]. The B site can improve the phase stability by altering the length of B-X bond [22]. X anion will influence the bandgap and stability of perovskites [23,24]. Therefore, the optoelectronic properties of metal halide perovskites can be effectively modified by altering the A, B, or X sites for specific applications. At room temperature, perovskites can be transformed into a tetragonal or orthorhombic crystal phase structure by adjusting the A, B or X ions (Fig. 1a). However, the formation of perovskite structures must strictly follow Goldschmidt's rules for tolerance factor (t) and octahedral factor (μ) [25]. For most perovskites, the value of t and μ are in the range of 0.8–1.1 and 0.44–0.90 [26], respectively, as shown in Fig. 1b. The most desirable crystal structure of perovskite is the cubic symmetric *Pm3 m* space group, where the octahedral corner-sharing $[BX_6]^{4-}$ surrounds A cation with 12-fold coordination [27].

Metal halide perovskites possess a favorable set of photophysical properties suitable for optoelectronic applications. They exhibit a very high absorption coefficient ($>10^5$ cm^{-1}) in the visible region [28]. Meanwhile, metal halide perovskites are bipolar charge transporters [29], and the carrier diffusion length can exceed 1 μm [3], which has a decisive impact on high efficiency devices. At present, according to the crystal properties, PODs can be classified into two types, namely, single crystal and polycrystalline thin films, respectively. Compared with polycrystals, perovskite single crystals have extremely low bulk trap densities, such as grain boundaries (GBs), which are several orders of magnitude lower, while the carrier diffusion length is about 100 times longer [30]. Therefore, in theory, single crystals outperform polycrystalline thin films in photoelectronic fields. However, the reality (so far) is different. For example, the best performance of perovskite polycrystalline thin films has been achieved in SCs, while there are only a handful of reports on single crystals, and most devices have efficiencies of less than 20%. Moreover, their synthesis and device integration are complex, and it is difficult to obtain large-area, thin and light PODs, which makes the road to commercialization very long. In contrast, polycrystalline devices which are easier to fabricate have demonstrated excellent performance. However, it is necessary to address the defect issues to further improve devices efficiency. Therefore, in this review, we mainly focus on polycrystalline thin film PODs, where defects can be divided into bulk defects inside perovskite and defects at GBs/interfaces. The most important technique for preparing polycrystalline thin film PODs is the solution method because of its low cost, simple process and abundant precursor materials [31]. Furthermore, many important parameters of perovskite films, such as surface coverage, grain size, crystallinity and defect density, are closely related to this fabrication technique [32]. During device fabrication, high defect density and carrier transport barrier always exist at the interfaces, resulting in large deviations from the ideal epitaxial heterostructure. The heterointerfaces are characterized by lattice mismatch, interface defect states, and band bending, all of which affect carrier dynamics. Therefore, defect engineering must be considered in PODs to improve their performance and stability.

Given the importance of defect engineering as described above, this manuscript provides a comprehensive review and summary to address some of the important advances reported to date from the extensive literature trove. This review aims to explore various strategies applied to PODs. Although these devices are used in different fields, they share many features and are governed by the same underlying physics. Therefore, many defect engineering strategies initially applied to one device can also be applied to other types to improve their optoelectronic properties. At the same time, a basic understanding of the similarities and differences between various PODs and their photophysical properties is crucial to tailor appropriate strategies for them. Therefore, after understanding how these engineering strategies can be applied to different perovskite functional layers (PFLs) and adapted to contact layers in different ways, this review would be helpful to provide new scientific insights for potential future directions, and pave the way for further commercialization in the field of PODs.

2. Defects in perovskite optoelectronic devices

2.1. Defects in perovskite materials

Ideally, every atom in a periodic lattice would be in its ideal position (Fig. 2a). However, perfect crystals do not exist. Due to the influence of crystal formation, atomic thermal motion and other conditions, the arrangement of atoms cannot be completely regular, and there are often regions that deviate from the ideal crystal structure. These deviations from the full periodic lattice structure are

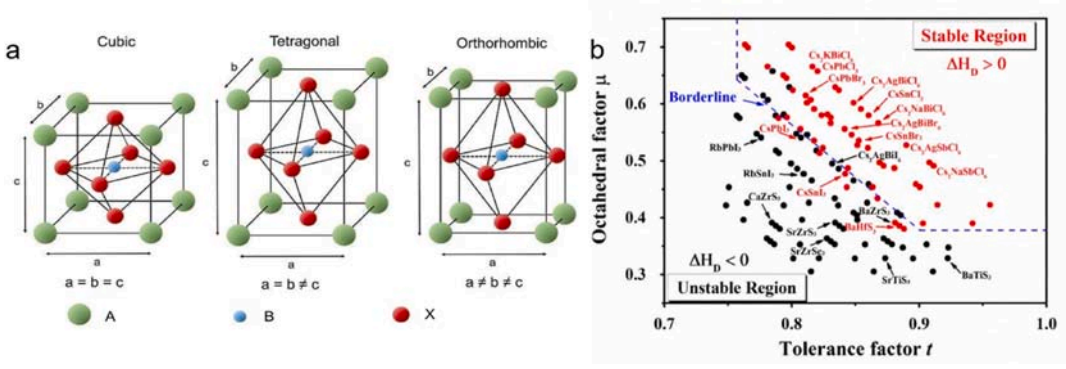

Fig. 1. (a) Crystal structure of metal halide perovskites. (b) Theoretical calculation of the tolerance factor μ for metal halide perovskites. Reproduced with permission from Ref. [26]: Copyright 2017, American Chemical Society.

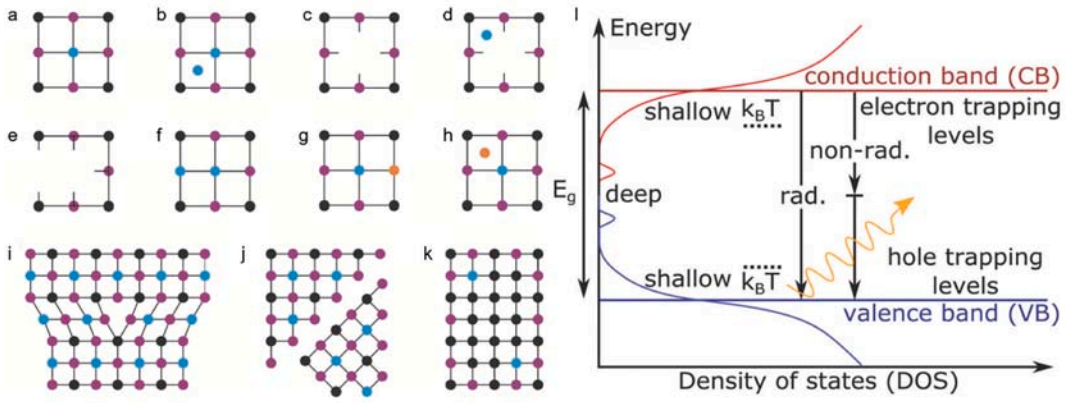

Fig. 2. (a) Illustration of perfect lattice (blue, black, and purple dots represent the A, B, and X site ions, respectively). (b) Vacancy. (c) Interstitial. (d) Antisite substitution. (e) Frenkel defect. (f) Schottky defect. (g) Substitutional impurity. (h) Interstitial impurity. (i) Edge dislocation. (j) Grain boundary. (k) Precipitate. Reproduced with permission. Reproduced with permission from Ref. [33]: Copyright 2018, John Wiley and Sons. (l) Schematic representation of the defect density of state in pervoskites, whereby both band-to-band radiative (rad.) and non-band-to-band non--radiative (non-rad.) recombination (vertical arrows) can occur. Reproduced with permission from Ref. [45]: Copyright 2016, Royal Society of Chemistry.

defects in the crystal, as shown in Fig. 2b–k, which break the symmetry of the crystal. Defects in conventional semiconductors have been studied extensively [33], and mainly classified into the following three types according to the distribution range of disordered arrangement.

2.1.1. Point defects

Point defects only involve lattice defects in the atomic size range. In ionic crystal, at a certain temperature, lattice atoms not only vibrate near the equilibrium position, but also gain enough energy to overcome the binding of surrounding atoms and squeeze into the gaps between the lattice atoms to form interstitial atoms (Fig. 2b), the original positions become vacancies (Fig. 2c). At this time, interstitial atoms and vacancies appear in pairs, called Frenkel defects (Fig. 2d). When only vacancies form in the crystal without interstitial atoms, they become Schottky defects (Fig. 2e). On the one hand, interstitial atoms and vacancies are continuously generated, and at the same time, the two are gradually recombined, and finally an equilibrium concentration is established. The above two temperature-dependent point defects are also called as thermal defects, and they always exist at the same time. Atoms must have larger energies to squeeze into interstitial sites, and their migration activation energy is smaller, so there are many more vacancies in crystals than interstitial atoms, which leads to vacancies being the most common point defects. If impurity atoms can directly replace intrinsic ones, such defects are called anti-site substitutions (atoms occupy the wrong sites in the lattice, as shown in Fig. 2g), also known as anti-structural defects. It should be noted that anti-substitution and interstitial atoms can exist in the ionic crystals like perovskites. However, the entire ionic crystal must remain electrically neutral. The type of defects in an ionic crystal depends on the composition of the ionic crystal, the relative size of the ions, and the number of charges carried by the ions.

2.1.2. Line defects

A line defect is a defect formed due to the abrupt termination of atomic planes in a crystal, as shown in Fig. 2i. The boundary between the slip part and the non-slip part in the crystal becomes the dislocation line. It can be clearly seen that the atoms surrounding the dislocation line are significantly displaced from their equilibrium positions, thereby dislocating the atoms above and below the dislocation line. The atoms above the dislocation line are squeezed, while the atoms below are stretched, so that the atoms above and below the dislocation line are subjected to compressive and tensile stress, respectively. Since the bonds around the dislocation line are stretched and squeezed, there is a strain field around the dislocation line.

It takes 100 eV of energy to create a 1 nm dislocation line, and a few eV of energy to create a point defect several nanometers long. Therefore, point defects are much easier to form than dislocations.

2.1.3. Planer defects

Many materials are polycrystalline, that is, consist of many small crystals with different orientations. Crystal junctions with different orientations are called GBs. Due to the sudden change of crystal orientation at the GBs, the atoms around the GBs obviously cannot meet their bonding requirements, resulting in the existence of vacancies, elongated bonds and dangling bonds at the GBs. In addition, there are some mismatched atoms on both sides of the GBs that are not arranged in the lattice. Atoms at GBs have higher energies than atoms inside a crystal, and elongated chemical bonds are more likely to break due to the presence of vacancies. Therefore, it is easier for atoms to diffuse along the GBs. In polycrystalline materials, impurities generally tend to accumulate in the GBs region. Due to the presence of vacancies and mismatched atoms in the GBs region, the atomic arrangement at the GBs is considered to be disordered.

The types of defects can be classified into shallow-level defect states (SLDS) and deep-level defect states (DLDS) according to their energy levels. Usually, SLDS are dominated by point defects, such as vacancies, interstitials, and anti-site substitutions, whose energies are in the range of tens of meV below the minimum of conduction band (CBM) or above the maximum of valence band (VBM), and the bound carriers with sufficient thermal energy can easily escape [34]. However, high-dimensional defects (dislocations, GBs, and precipitates) create DLDS, which are usually located in the middle of the bandgap. Importantly, the generation of defect states may take place not only during the perovskite synthesis, but also the PODs operation. For example, $MAPbI_3$ undergoes photodecomposition and thermal degradation when exposed to light [35,36]. Two reaction pathways are identified for the degradation. One leads to the irreversible decomposition of organic volatile gas species ($CH_3I + NH_3$), and the other to reversible decomposition (CH_3NH_2+HI), which can back react with PbI_2. The complete depletion of volatile organic components leads to a layer of PbI_2 on the perovskite film. Further decomposition of PbI_2 proceeds with reversible generation of I_2 and non-volatile metallic-Pb (Pb^0) under illumination or mild heating conditions. Several X-ray photoelectron spectroscopy (XPS) studies report the existence of Pb^0 [37]. Very likely these Pb^0 species exist at the surface or grain boundaries of perovskites, possibly as a core–shell structured cluster [38]. Recent reports claimed that sub-grain twinning domains in perovskites, although the number of experimental observations is still scarce [39–41]. The generation of such twins spontaneously forms triple (tetragonal/cubic/tetragonal) and double (tetragonal/cubic) stacked sequence layers, affecting the charge carrier transport properties [42,43]. The wave functions of these states are highly localized. Once the carriers relax to these DLDS, they need higher energy to become free carriers again [44], which is very difficult. Fig. 2l shows the location and the corresponding recombination of the two types of defects in perovskite [45]. Defects can also be distinguished into radiative and non-radiative recombination defects according to electron transition, ie, presence or absence of luminescence. Generally, SLDS restrict the effective movement of free carriers only through trapping and detrapping processes, while DLDS hinder detrapping and promote non-radiative recombination paths. Therefore, they affect the charge transport and optoelectronic properties of perovskite thin films, ultimately impairing the performance of PODs. Although Du et al. have demonstrated that DLDS are not dominant in perovskite films [46], according to theoretical calculations, that is, most of the defects in perovskite films are shallow point defects. The effect of point defects on PODs performance was further demonstrated by Angelis et al. [47], who reported that iodine defects reduce the trapping activity and largely affect the optoelectronic properties of perovskites. Du believes that only the iodine vacancies (V_I) and their antisite substitutions (such as I_{MA}) can induce deep electron and hole trapping levels, acting as non-radiative recombination centers.

2.2. *Defects at the interfaces*

For most PODs, the typical structure consists of transparent conductive oxide electrodes (i.e., indium tin oxide or fluorine-doped tin oxide)/electron transport layer (ETL)/PFL/hole transport layer (HTL)/metal electrodes (e.g., gold, silver, and copper), which contain four interfaces as shown in Fig. 3a. Charge extraction often occurs at these interfaces, so they play a decisive role in the performance of PODs. However, it is worth noting that the heterointerfaces between the perovskite and the adjacent contact layers (ETL or HTL) are more important because several physical processes (band bending, carrier injection, carrier recombination, charge accumulation, ion migration, *etc*.) occur at these interfaces will have a more direct impact on device performance [48], as shown in Fig. 3b. Time scales of charge dynamics are shown with arrows in different colors: (1) photogenerated excitons dissociate into free carriers; (2) charge diffusion from perovskite to interfaces (1 ps–1 ns); (3) charge extraction into ETL and HTL driven by interfacial electric field (<100 ps); (4) charge recombination induced by interface defect states (1 ns–1 ms); (5) reverse charge transfer at the interface (1 ms–1 s); (6) charge accumulation caused by ion migration (>1 s) [40]. It has been reported that interface defects, imperfect energy level alignment (ELA), and interface reactions should be the main reasons for the charge loss at the ETL/PFL and PFL/HTL interfaces [34,48,50–52]. Most of the defects at heterointerfaces (surface defects, GBs defects, precipitation defects, second-phase, *etc*.) are high-dimensional defects which are usually DLDS [53]. It is worth mentioning that surface termination is unavoidable during crystal growth and

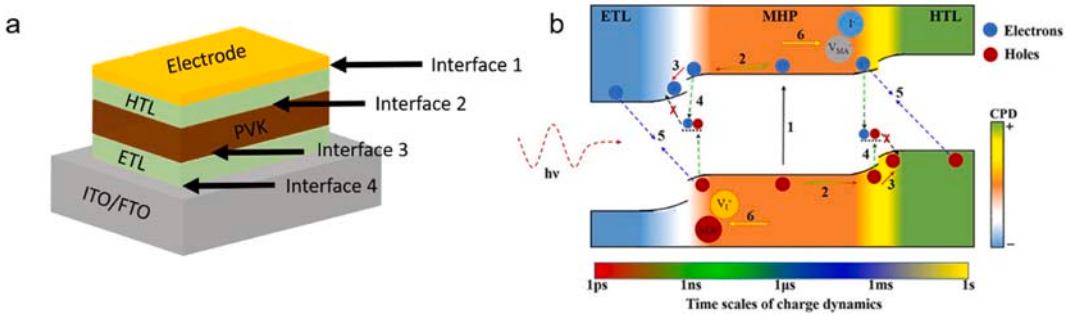

Fig. 3. (a) Schematic diagram of the defect distribution within perovskite optoelectronic devices. (b) Interfacial charge dynamics describing charge extraction, transfer, and recombination processes. Time scales for charge dynamics are displayed by different colors. 1) photo-generated excitons dissociate into free carriers; 2) charge diffusion from central to interface (1 ps–1 ns); 3) charges extraction into ETL and HTL driven by interfacial electric field (<100 ps); 4) charge recombination induced by interface defect states (1 ns–1 μs); 5) back charge transfer at the interfaces (1 μs–1 ms); 6) charge accumulation induced by ion migration (>1 s). The relevant timescales for above six charge dynamic processes were measured based on time-resolved microwave conductivity and transient absorption spectroscopy techniques. Reproduced with permission from Ref. [49]: Copyright 2018, John Wiley and Sons.

post-treatment. For example, two different terminations which are stable at room temperature have been proposed in the (001) $MAPbI_3$ surface: PbI_2 and MAI-terminated surfaces [54,55]. The surface of $MAPbI_3$ shows a larger bandgap compared to its bulk material. On MAI terminated surfaces, MA vacancies (V_{MA}) are easily formed due to the low formation energy (that is, the high volatility of MA^+). However, V_{MA} does not lead to DLDS, which means that few carriers will be trapped on the MAI terminated surface regardless of sample preparation conditions. Yu et al. reported that the charge defect density at the interface of polycrystalline thin films is 1–2 orders of magnitude higher than that the interior of the thin films [56]. Therefore, compared with defects in perovskite materials, non-radiative recombination induced by defects at the heterointerfaces is a predominant loss mechanism affecting the performance of PODs.

It is needed to consider that the SLDS will form at the termination of perovskite materials, and the defects will diffuse to the surface or GBs of the perovskite thin films on a slower time scale [57]. Then, the carriers trapped by the defects and ions migrated from the perovskite to the surface or GBs will accumulate at the interface, which results in band bending, change the energy level alignment and built-in electric field, *etc*. They are not conducive to carrier separation and injection, as well as transportation, and the performance and stability of PODs are ultimately reduced [52,58].

Meanwhile, the imperfect interface ELA is proven to be one of the important reasons for the loss of PODs performance. A perfect ELA (matched energy level) not only facilitates efficient charge extraction, transfer and collection, but also reduces interface charge accumulation. It has been reported by Qi et al. that ELA is affected by many factors, such as the energy level of adjacent interface materials, interface defects, ion migration, instability, and even the preparation conditions and substrates of the perovskite thin films [48].

Furthermore, the chemical reaction at the interface is another important reason for the severe degradation of PODs [52]. Interfacial reactions are caused by direct chemical reactions between adjacent interface materials or chemical reactions between ions or impurities in the PFL, ETL, HTL, or electrodes. It is well-known that vacancies can facilitate ion migration, and ions migrate much faster on the surface or GBs that in the thin films. This accelerates the chemical reaction between the interfaces, which in turn degrades the performance of PODs.

The defect density is one of the determinants of devices performance. Therefore, experimental conditions such as atmosphere (N_2 or air) and annealing procedures (temperature or time) must be precisely controlled to reduce defects. Ginley and Cahen et al. [59] first proposed the concept of "defect tolerance" to represent the low density of defects and the insensitive nature of defects. Although defects cannot be completely eliminated, the performance of PODs will only decrease when the defects density exceeds a certain value. Therefore, it is crucial to employ defect engineering to reduce the density of defect states in PODs.

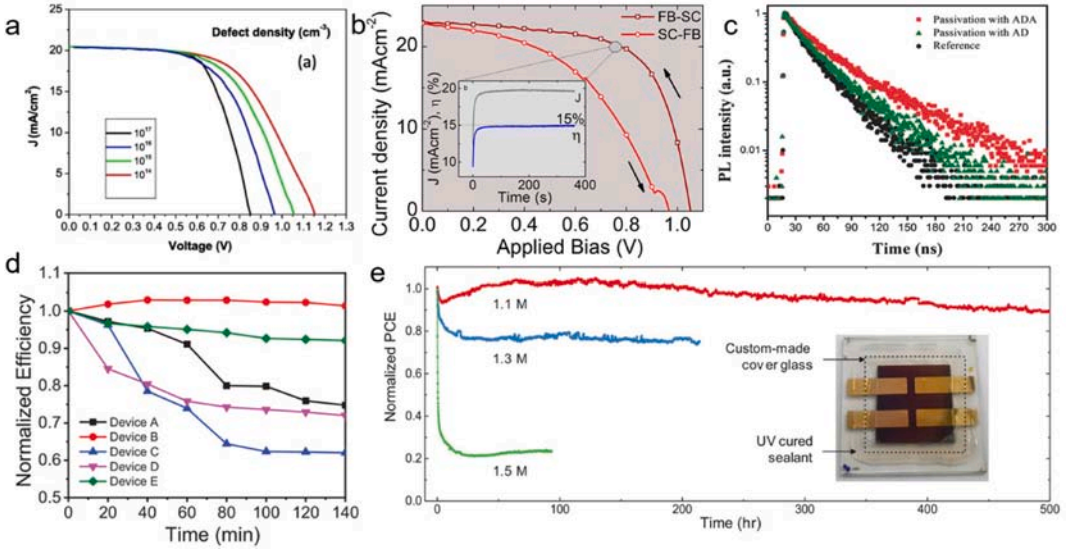

Fig. 4. (a) Theoretical (SCAPS) effect of different defect densities in *J-V* curves of a perovskite solar cell. Reproduced with permission from Ref. [64]: Copyright 2020, Elsevier. (b) The *J-V* curve of device shows a severe hysteresis. Reproduced with permission from Ref. [65]: Copyright 2014, American Chemical Society. (c) TRPL spectra of perovskite films before and after passivation by AD and ADA molecules with optimum concentration of 1.5 mg mL^{-1} in CB. Reproduced with permission from Ref. [66]: Copyright 2018, John Wiley and Sons. (d) Correlation between defect evolution and efficiency stability. Defect density versus normalized efficiency of the cells under different aging conditions and time under both illumination and bias voltage, under bias voltage and dark, under illumination and 0 V voltage. Top panel: bulk defect, bottom panel: interface defect. Reproduced with permission from Ref. [68]: Copyright 2019, John Wiley and Sons. (e) Time evolution of normalized PCEs of PSCs with different PbI_2 concentrations under 1-Sun illumination. All PSCs were glass-encapsulated using UV-resin. Reproduced with permission from Ref. [69]: Copyright 2021, John Wiley and Sons.

3. Effects of defects on perovskite optoelectronic devices

3.1. Solar cells

Key factors for evaluating the performance of perovskite SCs include open circle voltage (V_{OC}), FF, and short-circuit (J_{SC}), which are all directly related to incident photon-to-current conversion efficiency (IPCE). IPCE is determined by the charge extraction efficiency, which is given by the equation [60].

$$\mathrm{IPCE} = \eta_{\mathrm{LHE}} \times \eta_{\mathrm{inj}} \times \eta_{\mathrm{cc}} \tag{1}$$

where η_{LHE} is the light-harvesting efficiency, η_{inj} is the charge extraction (injection) efficiency, and η_{cc} is the charge collection efficiency. Furthermore, the charge extraction efficiency is defined as [61].

$$\eta_{\mathrm{inj}} = \frac{k_{\mathrm{inj}}}{k_{\mathrm{inj}} + k_{\mathrm{r}} + k_{\mathrm{nr}}} \tag{2}$$

where k_{inj}, k_{r}, and k_{nr} are the injection, radiative recombination and non-radiative recombination rate, respectively. Therefore, to achieve higher IPCE, it is necessary to maximize the injection rate while minimizing the other two constants. k_{inj} dependents on the ELA associated with the contact material, while k_{r} and k_{nr} are sensitive to the crystal and interface quality. For perovskite materials, k_{r} (10^{-9} s^{-1}) is much slower than k_{nr} (10^{7} s^{-1}) [62], so while providing sufficient driving force for charge injection, it is more important to reduce interface defects that can cause non-radiative recombination. Non-radiative recombination also affects the steady-state carrier density and thus the quasi-Fermi level splitting, which is related to V_{oc} as described by the following equation [63].

$$V_{\mathrm{oc}} = \frac{kT}{q} \ln\left(\frac{J_{\mathrm{ph}}}{J_0} + 1\right) \tag{3}$$

where q is the elemental charge, k is the Boltzmann constant, T is temperature, J_0 is the saturation current density, and J_{ph} is the photocurrent density. The influence of different defect densities on the *J-V* characteristics of perovskite SCs are presented in Fig. 4a, and it can be easily found that the defect density has a significant effect on V_{oc}. As an interesting result, it is observed that the defect density increases from 10^{14} to 10^{17} cm^{-3}, V_{oc} decreases from 1.15 to 0.85 V, while J_{sc} is not affected by defect density in this range [64]. More importantly, the charge accumulated at the interface can generate capacitive current through the charge trapping/de-trapping processes, which is the main reason for the notorious *J-V* hysteresis (Fig. 4b) [65]. Moreover, the defect density affects the diffusion length of carriers, which can be determined by the photoluminescence (PL) lifetime. In Fig. 4c, Grätzel et al. treated perovskite thin films with adamantane (AD) and 1-adamantylamine (ADA), and they found that the emission lifetime becomes longer after treatment [66].

Last but not least, defect density plays a key role in the degradation of perovskite SCs [67]. Defects may facilitate the passage of

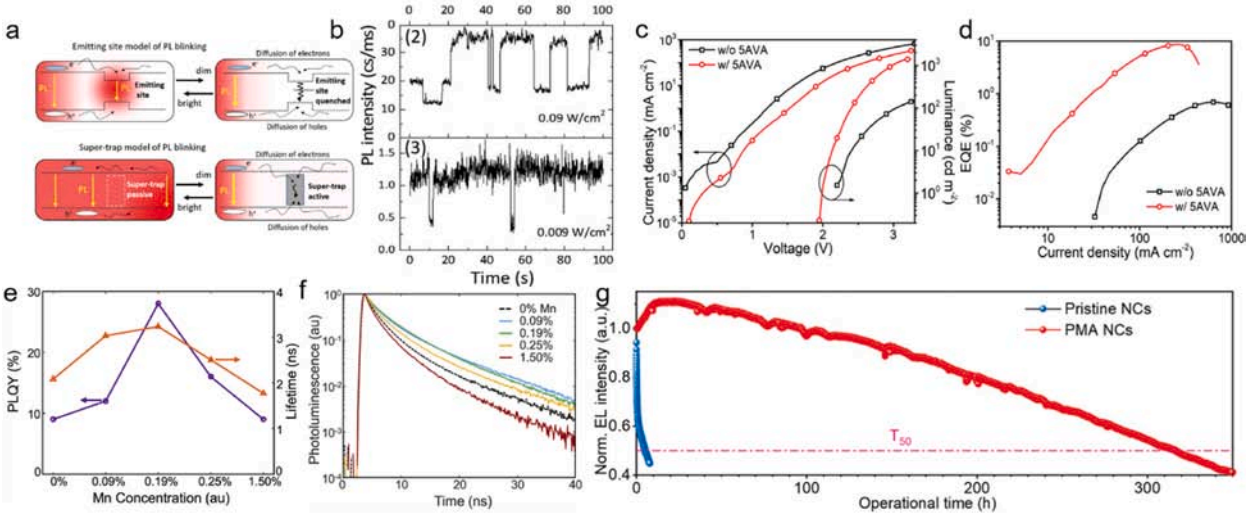

Fig. 5. (a) Proposed blinking mechanism due to ion migration caused by defects. (b) PL transients obtained at different excitation power densities. Reproduced with permission from Ref. [75]: Copyright 2021, John Wiley and Sons. (c) Current density-voltage (*J–V*) and luminance-voltage (*L–V*) curves. (d) EQE-current density curves of NC-LEDs. Reproduced with permission from Ref. [78]: Copyright 2019, American Chemical Society. (e) Fluence-dependent PLQY. (f) TCSPC probed PL lifetime. The excitation density for the TCSPC measurement is around 10^{15} cm^{-3}. Reproduced with permission from Ref. [79]: Copyright 2019, Elsevier. (g) The operational lifetime of the $CsPbI_3$ perovskite LEDs at a constant current density of 30 mA cm^{-2}. Reproduced with permission from Ref. [81]: Copyright 2021, John Wiley and Sons.

oxygen or moisture through PFL, and accelerate the degradation of perovskite SCs under ambient conditions, which would seriously hinder the commercial application. Meng and co-workers summarized the relationship between the defect density and the normalized efficiency of these SCs under different aging conditions and times [68]. As shown in Fig. 4d, regardless of the aging conditions, there is no obvious correlation between efficiency stability and bulk defects. In contrast, a decrease in efficiency is always accompanied with the increase of interface defect density. Therefore, they concluded that the increase in interface defect density caused by voltage may be the source of stability problems. In this case, lighting can speed up the effect by altering the charge distribution or providing excess charge in the SCs, especially at the interface. Fig. 4e also suggested passivation of the Pb–I related antisite defects near the GBs and the interface is crucial for the fabrication of SCs with enhanced long-term stability.

3.2. Light-emitting diodes

For perovskite LEDs, one of the problems is the blinking phenomenon [70–72]. At present, there are mainly two explanations for this. One is the non-radiative Auger recombination related to the combination of the charge trapped in the defect states with another exciton [73]. The another is the activation and deactivation of defect states as PL quenchers [74]. Whatever the cause, blinking phenomenon is closely related to defects. In addition, defects are also a major source of ion migration. Defects that are non-radiative recombination centers can migrate by ion transport. Therefore, the position of radiative and non-radiative recombination can change with each other (Fig. 5a), further leading to significant deviations in the PL intensity of the perovskite thin films over time [75].

The most important indicator for evaluating LEDs performance is EQE, which is defined as the number of photon emitted from the diode/the number of electrons injected into the diode, and is given by [76].

$$\eta_{EQE} = \gamma \cdot \varepsilon \cdot \varphi \tag{4}$$

where γ is the out-coupling factor, ε is the charge balance factor, and φ is the quantum efficiency. There is no doubt that the charge injection and transport properties are directly determined by the number of defect states. In addition, they are also affected by the charge carrier mobility of ETL/HTL, which is also determined by defect states. Therefore, a suitable interface layer is of great significant for ε of LEDs and their efficiency. Another issue to consider is the ELA. The charge carriers must have sufficient energy to overcome the energy barrier created by the difference between the work function of the metal electrode and CBM (for electron injection) or VBM (for hole injection) of the semiconductors. According to the Fowler-Nordheim tunneling theory, the relationship between current and energy barrier is as follows [77].

$$J \propto E^2 \exp\left(-\frac{\Delta}{E}\right) \tag{5}$$

where J is the current density, E is the electric field, and Δ is a barrier shape related parameter, determined by [77].

$$\Delta = \frac{8\pi\sqrt{2m^*}h^{\frac{3}{2}}}{3q\hbar} \tag{6}$$

where h is the barrier height, q is the elemental charge, $\hbar$ is reduced Planck's constant, and m^* is the effective mass of charge carrier. Generally, the turn-on voltage is determined by the flat-band condition, which is governed by the work functions of anode and cathode. And the operating voltage is related to the barrier height and the charge injection characteristics of majority carriers. The efficiency (η) is defined by [77].

$$\eta \propto \exp\left(-\frac{ah^{\frac{3}{2}}}{V}\right) \tag{7}$$

where a is a constant and V is the applied bias. It is easy to find that small energy barriers for majority and minority charge injection are essential for high EQE and low operating voltages of perovskite LEDs. Energy level matching at the interface is very important to achieve efficient charge injection and recombination, as well as high operational stability, since inefficient charge injection can lead to charge imbalance and accumulation of space charges.

As shown in Fig. 5c and d, Wang et al. reported that LEDs treated with 5-aminovaleric acid (5AVA) had higher current densities and significantly improved EQE [78]. A maximum EQE of 8.7% at a current density of around 1408 cd m^{-2} and an emission wavelength around 662 nm was measured, placing these red perovskite LEDs in the same quantum efficiency range as commercial organic LEDs. Moreover, Cogreve et al. increased the emissive lifetime and photoluminescence quantum yield (PLQY) while reducing the defect states, as reflected in a slight reduction of Urbach energy [79] (Fig. 5e and f). And Gao et al. significantly enhanced interaction with defect sites and minimized non-radiative recombination losses by weakening the hydrogen bonds between passivating functional moieties and organic cation in perovskite [80]. Excellent defect passivation results in a significant reduction of defect states in 2, 2'-(ethylenedioxy)diethylamine (EDEA)-treated perovskites. The PLQY of the device is greatly improved over a wide range of excitation densities, with a peak PLQY of 56%. Even at a low energy density of 0.02 mW/cm^2, the EDEA-treated films maintain a high PLQY of 40%, consistent with the low defect density. Low defect-mediated recombination in the EDEA-treated samples is also confirmed by the time-correlated single-photon counting (TCSPC) measurements, which shows a prolonged PL lifetime of 1330 ns, compared to the control (130 ns) and hexamethylenediamine (HMDA)-treated films (690 ns).

Finally, the issue to be considered is stability. To address this issue, Choy and co-workers used poly(maleic anhydride-*alt*-1-octadecene) (PMA) to passivate defects in perovskite LEDs, and the results are shown in Fig. 5g. Due to the passivation, the PMA treated thin film showed a superior operational stability with a greatly extended T_{50} of 317 h at a constant current density of 30 mA cm^{-2} [81]. It should be noted that there is a gradual increment in the first 10 h. Such increasing performance can be attributed to the defect self-healing behavior under electric fields.

3.3. Field effect transistors

FETs can amplify or switch electronic signals by changing the electric field. They are the cornerstone of microelectronics and are widely used in computers and other electronic applications. An illustration of transport mechanisms and energy landscape of the charge defects was proposed by Weitz et al. as shown in Fig. 6a [82]. In the dark (left), the gate induces a low density of charge carriers. Since only a small fraction of the defects are filled, thermal activation of DLDS dominates the transport. However, in the illuminated samples (right), a high density of photoexcited charge carriers is generated and the DLDS are completely filled. In this case, only SLDS affect charge transport at high temperatures. At low temperatures, SLDS also freeze, enabling phonon-limited transport. Relative to DLDS, this charge transport tolerance in the bright state is remarkable. The suppressed effect of DLDS can also be seen as an extension of "defect tolerance" in perovskite materials, which so far has only been associated with the presence of SLDS.

Generally speaking, the performance of FETs can be characterized by a number of important metrics, including field effect mobility (μ), on/off ratio (I_{on}/I_{off}), threshold voltage (V_0), and sub-threshold swing (SS). Apparently, μ is the most important parameter to evaluate FETs, and it is mainly used to characterize the carrier transport capability. The following equation can be used to extract the FET transfer characteristics from different regions [83].

$$\mu = \begin{cases} \dfrac{L}{C \times W \times V_{ds}} \times \dfrac{\partial I_{ds}}{\partial V_g}, \text{for the linear region} \\ \dfrac{2L}{C \times W} \times \left(\dfrac{\partial \sqrt{I_{ds}}}{\partial (V_g - V_{th})} \right)^2, \text{for the saturation region} \end{cases} \tag{8}$$

where L is the channel length, C is the gate-channel capacitance, W is the channel width, V_{ds} and I_{ds} are the source-drain voltage and current, respectively, V_g is the gate voltage, and $V_{th} = V_g$-V_{ds} is the threshold voltage. Another important parameter is I_{on}/I_{off}, which can be calculated from the ratio of the drain current in the on and off states. This parameter describes the ability to control the channel current through the gate bias, so for higher quality devices, this value should be as large as possible. $SS = \partial V_g/\partial(\log I_{ds})$ represents the speed capability of the device to switch between on and off states [84].

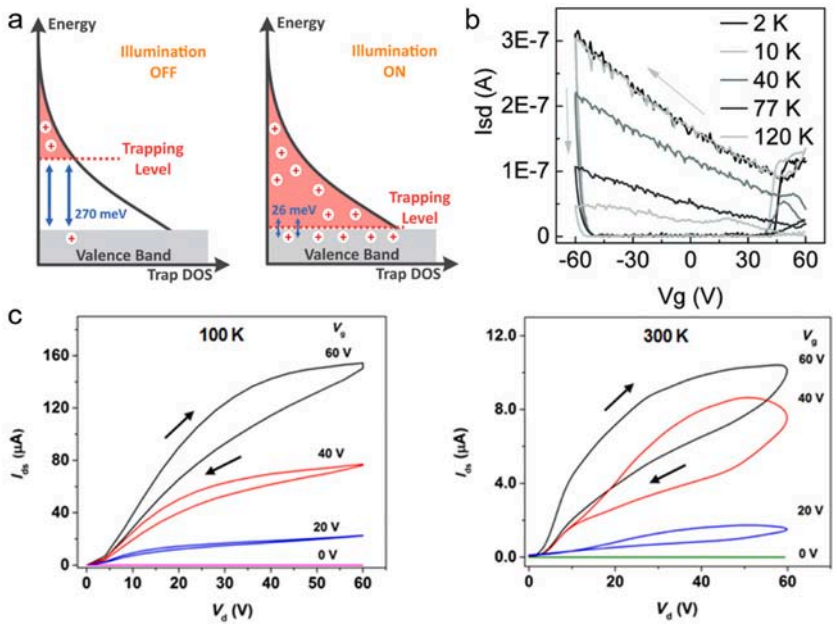

Fig. 6. (a) Schematic trap density of state with the trap filling level (red) for dark (left) and illuminated (right) samples. Reproduced with permission from Ref. [82]: Copyright 2021, John Wiley and Sons. (b) The temperature dependent transfer characteristics of the BN covered FETs after 3 min annealing at 120 °C. The source-drain voltage is 20 V. Reproduced with permission from Ref. [88]: Copyright 2016, John Wiley and Sons. (c) Output characteristics of FETs with PEIE-treated Au S-D contacts at 100 and 300 K, respectively (L = 20 μm and W = 1 mm). Reproduced with permission from Ref. [87]: Copyright 2017, American Association for the Advancement of Science.

Similar to perovskite SCs and LEDs, FETs suffer from ion migration. Halogen vacancies and organic cation vacancies have relatively small activation energies, leading to the existence of ion migration [85,86]. According to the previous reports, the diffusion coefficient of iodine vacancies decreases by a factor of 10^5 from room temperature to 100 K, and the ion migration is almost suppressed when temperature is below 240 K [87]. Therefore, the process of ion migration to create defects is strongly temperature-dependent. When a negative (positive) gate voltage is applied, the positive (negative) ions drift to the interface with the dielectric layer at room temperature, and the oppositely charged vacancies will move in the opposite direction. This shields the applied gate electric field and reduces the concentration of mobile holes in the carrier transport channel, resulting in low carrier mobility. Meanwhile, the accumulation of ions at the perovskite/dielectric interface also hinders the further injection of charged carriers [12]. Furthermore, these defects can trap carriers during operation, thereby degrading the performance. In Fig. 6b, it is noted that conventional three dimensional (3D) perovskite FETs lose their transistor characteristics at room temperature, which is mainly due to serious ion migration [88]. In addition, the hysteresis reported in perovskite FETs is also resulted from the ion migration. Due to the thermal dependence of ion migration, the hysteresis effect is more severe at high temperatures (above 240 K) than at low temperatures (below 240 K) (Fig. 6c) [87]. At room temperature, ions and ionic defects migrate under the bias voltage, resulting in more severe hysteresis. This phenomenon not only leads to inaccurate carrier mobility, but further limits the performance of devices.

3.4. Lasers

Optical gain, that is, population inversion, is a fundamental requirement for lasing, because light amplification by stimulated emission is only possible when there is population inversion between two dipole-coupled electronic states. Population inversion is closely dependent on the dynamics of excited state charge carriers, because it relies on the extremely fast accumulation of excited state charge carriers, which can be disrupted by different recombination pathways such as defect trapping. In perovskites, the excited charge carrier dynamics after photoexcitation undergo decoherence, thermalization, polaron formation and cooling in CB within a fast timescale of 1 ps, followed by different recombination pathways. The carriers relax to VB, as illustrated in Fig. 7a [89,90]. For semiconductors, excited carriers exist in the form of electron-hole plasma, and the recombination kinetics are described by the following rate equation

$$\frac{dn}{dt} = -An - Bn^2 - Cn^3 \tag{9}$$

where n is the density of the excited carriers, t is the time, and A, B, and C are the rate coefficients corresponding to monomolecular defect-assisted recombination, bimolecular radiative recombination, and three-body Auger recombination, respectively [5,91]. To achieve population inversion, excited state carriers need to maintain their occupancies in CB to accumulate excited state carriers, and this process can be disrupted by non-radiative recombination pathways. Obviously, defect-assisted recombination should be suppressed because it is one of the two main non-radiative pathways. The stimulated emission occurs under high excitation intensities

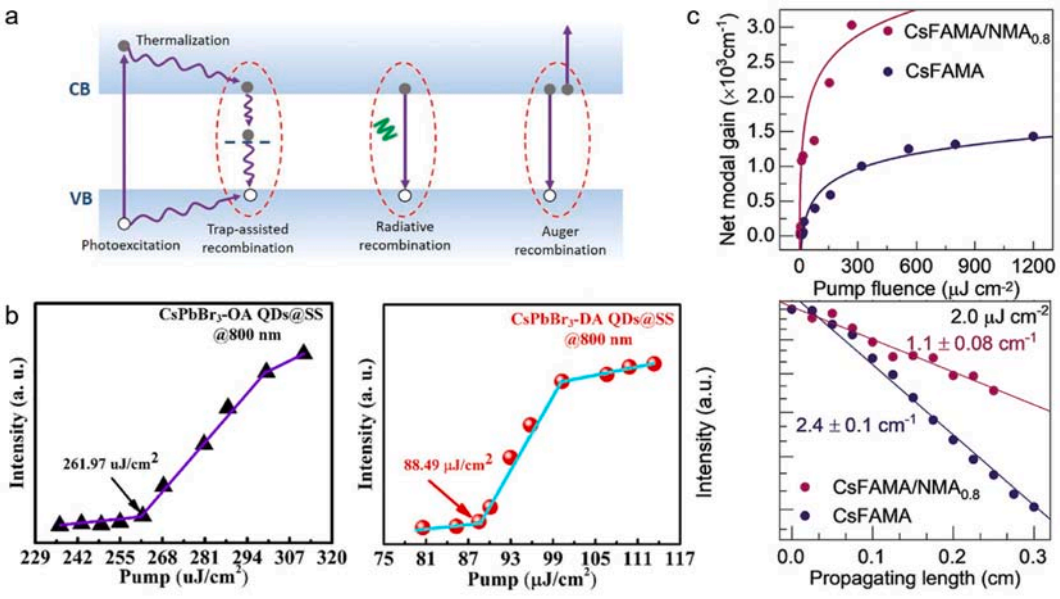

Fig. 7. (a) Schematic diagram of different recombination dynamics in perovskites. (b) The lasing threshold behaviors of both SiO_2 spheres coated with QDs of the oleic acid (OA) ligand and 2-hexyldecanoic acid (DA) ligand under 800 nm pumped laser. Reproduced with permission from Ref. [96]: Copyright 2020, Elsevier. (c) Gain (top) and loss (bottom) measurements of the $MAPbBr_3$-MAAc and $MAPbBr_3$-DMF:DMSO films. Reproduced with permission from Ref. [97]: Copyright 2021, John Wiley and Sons.

with a large density of excited carriers (up to 10^{17} cm^{-3}), where bimolecular radiative recombination competes with monomolecular defect-assisted recombination [92,93]. Second, the defect tolerance of perovskite results in a low bulk defect density [35,94], while surface defects, including GBs, have a long trapping time in the order of nanoseconds compared to the occurrence time of amplified spontaneous emission (ASE) within 10 ps [95]. In addition, passivation of defects on the thin film surface and GBs has been reported to lower the ASE threshold (Fig. 7b) [96].

Another way to evaluate the ASE performance of perovskite thin films is to measure their net gain and loss characteristics by the variable stripe length method, as shown in Fig. 7c. The output intensity of perovskite thin films increases exponentially with the length of excitation strip length, which can be expressed as [97].

$$I = \frac{A(\lambda)I_P}{G(\lambda)}\left[e^{G(\lambda)L} - 1\right] \tag{10}$$

where $A(\lambda)$ is a constant related to the spontaneous emission cross-section. I_p, $G(\lambda)$, and L are the pumped energy intensity, net gain coefficient, and pumped stripe length, respectively. In addition, the optical loss can be extracted by measuring the emission intensity as the excitation region moves from the edge of the film. Because the emission at the end of the pump stripe is constant, the signal detected from the film edge follows the Beer-Lambert law [98].

$$I = I_0 e^{-\alpha x} \tag{11}$$

where α is the waveguide loss coefficient, and x is the length of the unpumped region from the end of the pump region to the edge of the sample. In the paper reported by Zhang, according to the fitted lines in Fig. 7c, the loss coefficient as-fabricated mixed-naphthylmethylammonium (NMA) perovskite films is determined to be of 1.1 cm^{-1}, which is nearly two times lower than that of 2.4 cm^{-1} for CsFAMA film [97]. From a practical application point of view, low ASE threshold, high net mode gain, and low optical loss facilitate high-quality lasers. Therefore, defects control is important to achieve advanced laser performance.

4. Defects engineering

4.1. Passivation mechanisms

For metal halide perovskites, the concentration, types and energy level positions of defect states are determined by the enthalpy of their formation and the crystallization kinetics and dynamics, including the material stoichiometry, light exposure, temperature, atmospheric humidity and pressure. Compositional alloying has been shown to be an efficient approach to suppress defects in perovskites through phase separation into lower defect phases. Despite the overwhelming advantages in this respect of perovskites by virtue of enormous defect tolerance, their 'soft' crystal lattice and subsequent low defect formation energies are expected to introduce relatively large concentrations of defects, which are often detrimental to performance. Intrinsic (or native) point defects are commonly branded using Kröger-Vink notation, whereby label MS identifies both the defective species (M) and lattice site (S). Theoretical calculations including ab initio and density functional theory (DFT) methods provide one of the most powerful and direct tools for exacting the nature and origin of defects. This is because it is practically impossible for experimental probes to reliably provide an atomistic picture of the imperfection, and thus must be complemented via predictive materials modeling. The electronic band structure of perovskites is derived from the electronic Pb-X sub-lattice, and most defect states will be directly linked to the energy levels created at improper bonding at these respective sites. For an effective passivation, new chemical bonds formed on the Pb-X derived surface orbitals are pumped by appropriate dopants, allowing the defect energy levels shift toward or into the band edges, there reducing the negative influence of the defects. In addition, the effects of charged defects and specifically highly mobile ions have become an important research topic. This is because the migration of ionic defects with low activation energies forms an intrinsic mechanism inside perovskites, with the notable exception of Pb^{2+} migration (activation energy is generally considered too large). Consequently, this kind of defects are particularly influential in PODs, as they can easily diffuse through the perovskite crystal while exposed to an external bias. Charged defects are considered as the origin of elemental redistribution within perovskites and have been linked to local changes in density of states and electrical properties. While charged migrating ions themselves do not necessarily contribute to charge trapping, organic-inorganic perovskites are increasingly being considered as soft lattice, and such phenomenon contributes and complicates the environment in which defects form and influence carriers deep inside the crystal. In this situation, Lewis bases or acids are very strongly favorable.

As for the extrinsic defect states, they can mainly be divided into GBs and defects at the interfaces. Two dominant sources of extrinsic defects in metal halide perovskite thin films occur at the GBs and the terminating surface states, due to the widespread application of grainy spin coated thin films. Extrinsic surface defects caused by the surrounding environment or unsaturated surface bonds are the major concern in perovskites, as solution processed thin films often form grainy and polycrystalline networks. The kinds of defects that can form at GBs and on the surface of perovskites are far more varied than the intrinsic point defects found in the crystal bulk. The diversity of improper bonding options at GBs and surfaces increases the contribution of parasitic DLDS and nonradiative recombination losses. Rather than chemically passivating surfaces and GBs defect states, several morphology-based techniques have been developed to reduce their effect. For instance, solvent treatment during thermal annealing process can efficiently increase the crystallinity and grain sizes of $MAPbI_3$ and help seed homogeneous film grow across the substrate, resulting in an almost uninterrupted vertical grain formation [99]. For PODs, the defect states at the interfaces may show the heavier impact on the performance. Synergistic adoption of coordinate bond, ionic bond, and conversion into low-dimensional perovskite is an important research direction

toward eliminating detrimental defects at the surface and GBs of perovskite films. Besides, synergistic passivation of bulk and interface defects is also necessary for minimizing perovskite-related nonradiative recombination. ELA affects charge extraction, transport, recombination, and accumulation. Therefore, it is a feasible and effective approach for reducing or eliminating to modulate ELA, which always results in the hysteresis in SCs and FETs. Interfacial ELA can usually be modulated through wide-bandgap perovskites or wide-bandgap transport materials [100]. It is needed to emphasize that, in addition to their effects, the chemical interactions between the incorporated wide-bandgap perovskite interfacial layers and primary perovskites and/or HTLs should also be considered, since interfacial reactions are usually caused by the ions or molecules migration and/or diffusion of interfacial contact materials in PODs.

4.2. Dopants

A common route to passivate defects is to add dopants or additives to the perovskite precursor solution to minimize the formation of defects during the growth of the perovskite. Inorganic dopants such as I^{3-}, K^{+}, Ni^{2+}, Al^{3+}, Cs^{+}, and Rb^{+} ions, and organic dopants such as MA and 2,3,5,6-tetrafluoro-7,7,8,8-tetracyanoquinodimethane (F4TCNQ) are successfully applied in the precursor solution to passivate different types of defects densities [101]. Anions are always used to passivate lead interstitials and halide vacancies (Fig. 8a), because it can donate electron density to under-coordinated Pb atoms. For example, the doping of chloride ions promotes the growth of perovskite crystals and the passivation of GBs [102]. The report by Jung et al. shown that Br^{-} doping promotes the separation of electrons and holes [103]. As the most electronegative atom among all halides, F^{-} tends to form strong hydrogen bonds with organic cations and strong ionic bonds with Pb, and exhibits strong surface passivation through accumulation [104]. Other anions such as SCN^{-} and ionic liquids ($BMIMBF_4$) are also used to passivate defects in perovskites [105,106]. Ma et al. treated the perovskite thin films with SCN^{-}, and found that the PLQY of the perovskite thin films increased from 17.85 to 69.0% after adding 10% SCN^{-} [107]. Meanwhile, τ_{avg} increases from 166.7 to 281.0 ns. They also calculated the radiative recombination rate (k_{rad}) and the non-radiative recombination rate (k_{nonrad}). As a result, the k_{nonrad} value decreases from $3.20 \times 10^{6}\ s^{-1}$ (0% SCN^{-}) to $1.10 \times 10^{6}\ s^{-1}$ (10% SCN^{-}), and the k_{rad} value shows little difference, indicating that non-radiative channel is mainly caused by the defect-induced traps. While the introduction of SCN^{-} greatly passivate the defects. Based on this, the ASE threshold of the SCN^{-}-doped perovskite thin films is low, only 2.6 μJ cm^{-2}, which is much lower than 12.5 μJ cm^{-2} for the pristine films. Among the anion doping, the most controversial dopants is I^{-}. Some researchers have found that I_2 vapor can cause the instability in I-based perovskite devices [108]. They attributed the reason to the reaction between I_2 and the mobile ions in the perovskite. However, Seok et al. introduced iodide ion in precursor and found it could reduce the concentration of DLDS [6]. The added I^{3-} is considered as an internal passivation agent to reduce the compositional point defects. The best certified efficiency is up to 22.1% and to almost 20% for 1 cm^2 SCs with the addition of I^{3-}. The marvelous stability is reflected in over 93% of the initial PCE after 13 months at ambient conditions. This method shows that exploiting

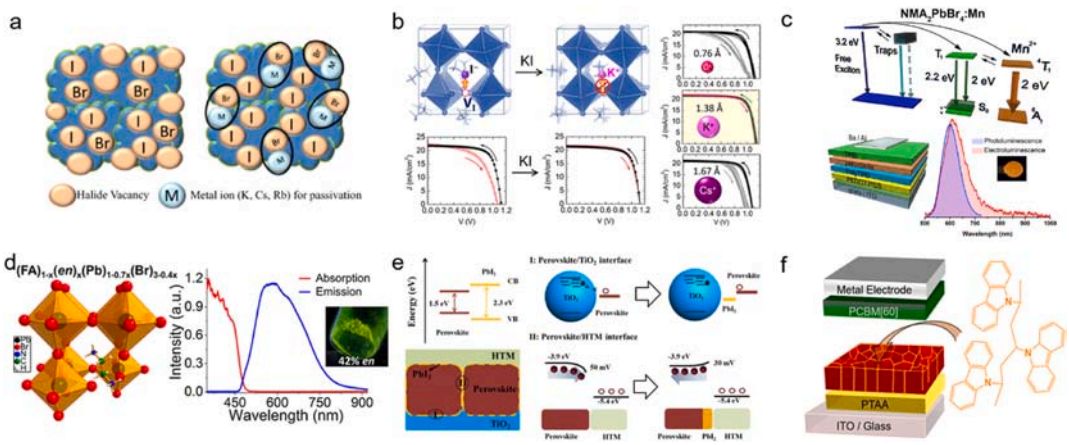

Fig. 8. (a) Schematic representation of halide vacancy in perovskite film which is passivated by coordination with metal (M) atoms at the grain boundaries and the perovskite surface. Reproduced with permission from Ref. [101]: Copyright 2020, IOP Publishing. (b) The *J-V* characteristics of perovskite SCs under 1 sun of illumination, doped with different alkaline metal iodides. Reproduced with permission from Ref. [109]: Copyright 2018, American Chemical Society. (c) Schematic representation of the energy-level diagram in the Mn-doped system. The blue levels represent the perovskite's excitonic transition. The light-blue levels represent permanent defects with a wide energy distribution, and the two arrows show radiative (continuous line) and non-radiative (dashed line) recombination processes. T_1 and S_0 (green levels) are the triplet and ground singlet state of NMA, respectively. The radiative transitions from T_1 to the two vibrational levels of S_0 (*v* and *v*'), with energy of 2.2 eV (560 nm) and 2.0 eV (605 nm), are represented. The orange levels represent the $^4T_1 \rightarrow {}^6A_1$ transition based on the 3d orbitals of Mn^{2+}. Reproduced with permission from Ref. [111]: Copyright 2019, Elsevier. (d) Structural derivation of the "hollow" perovskite from the proper 3D perovskite, and emission spectra of compounds $(FA)_{1-x}(en)_x(Pb)_{1-0.7x}(Br)_{3-0.4x}$ with an increasing amount of *en*. Reproduced with permission from Ref. [112]: Copyright 2021, American Chemical Society. (e) Proposed mechanism for PbI_2 passivation in $CH_3NH_3PbI_3$ films. The perovskite/HTL interface is described on the bottom right; the presence of PbI_2 changes the grain-to-grain boundary bending from downward to upward, which helps decrease recombination between the electrons from perovskite and the holes from HTL. Reproduced with permission from Ref. [128]: Copyright 2018, Elsevier. (f) Schematic diagram of PVC-treated SCs. Reproduced with permission from Ref. [131]: Copyright 2020, American Chemical Society.

the balance of halides in internal perovskite thin films is an effective way to fabricate highly efficient and stable devices.

Parrallel to the anions, positively-charged metal cations are used to passivate the I interstitial and Pb–I antisite substitutions. Park and co-workers found that doping with K^+ reduces the hysteresis of the *J-V* curve of perovskite SCs (Fig. 8b) in comparison to the other alkaline metal iodides, due to the lower formation energy of K-sites in $(FAPbI_3)_{0.875}(CsPbBr_3)_{0.125}$-based perovskite [98]. The device has a PCE of 17.14% at the reverse scan and 17.55% at the forward scan. It has been reported that divalent or trivalent dopants such as $Ni^{2+}$and Eu^{3+} can be used in the perovskite precursor solutions to passivate defects [110,111]. Wang et al. showed that Ni^{2+} suppresses the formation of Pb interstitials and Pb–I antisite substitutions through the distribution between MA cations or $[PbI_6]^{4-}$ octahedra [109]. A. Petrozza et al. investigated the effect of Mn^{2+} and Eu^{3+} doping in NMA_2PbX_4, where NMA = 1-naphtylmethylammonium (Fig. 8c) [111]. The luminescent efficiency is significantly improved (PLQY >22% in doped films). As shown in Fig. 8d, a new 3D highly defective but crystalline "hollow" bromide perovskites with general formula $(FA)_{1-x}(en)_x(Pb)_{1-0.7x}(Br)_{3-0.4x}$ (*en* = ethylenediammonium (en^{2+}), x = 0–0.44) was engineered [112]. When x > 0.33 *en* incorporation, the perovskite exhibites a strong broad light emission (1% PLQY) that persists after exposure to air for more than one year. Among the three trivalent cations, Eu^{3+} acts as a "redox shuttle" which oxidizes Pb interstitials and reduces I interstitials, thereby improving the performance and stability of PODs. Furthermore, adding appropriate cations, such as Cs^+, to form mixed A-site cationic halide perovskite structures can achieve improved stability and better performance. However, the structural changes and modifications to optoelectronic properties of these mixed-cation perovskites at the atomic scale are not fully understood. Islam et al. investigated the mixed cation system $FA_{1-x}Cs_xPbI_3$ using a combination of static and dynamic ab initio simulations [113]. They found the band gap widens with increasing Cs content in $FA_{1-x}Cs_xPbI_3$. And the alignment of frontier energy levels are also altered by the structural distortions. The symmetry-breaking distortions of the Pb/I lattice give rise to a Rashba-type effect, which spin-splits the frontier electronic bands making the band gap indirect, reducing the rate of charge-carrier recombination. Based on this, they selected seven different sized A-site cations with low concentrations to subsititute A-site cations, and indicated that all the cation substitutions increase the activation energy for iodide ion transport relative to pure perovksite [114]. The most important is partial guanidinium substitution can strongly suppresses ion transport. And Senanayak et al. investigated the mechanism behind operational instabilities and husteresis effects [115]. They showed that the incorporation of multiple cation using strain-relieving cations like Cs^+ and cations such as Rb^+ as passivation/crystallization modifier is an effective strategy to reduce vacancy concentration and ion migration in perovskite FETs. Based on this, these perovksite FETs achieve high performance with low hysteresis, high threshold voltage stability ($\Delta V_t < 2$ V over 10 h of continuous operation), and high mobility values > 1 $cm^2\ V^{-1}\ s^{-1}$ at room temperature.

In addition to defect passivation, B- and X-site ion doping may also lead to unexpected device performance. Smaller B-site doping was used to obtain highly efficient and thermally stable PODs by increasing the short-range order and reducing halide vacancies. $CsPb_{1-x}Cu_xX_3$ QDs were formed to achieve the blue-emitting LEDs, with a high PLQY of over 80% and a stable luminescence performance even under temperature over 250 °C [116]. And nickel ion (Ni^{2+}) is another alternative for improving the performance of perovskite [117]. It has been reported that Ni^{2+} has a strong preference for octahedral coordination with halide ions, which substantially removes structural defects, and results in improved short-range order of the perovskite lattice. Benefiting from this, the $CsPbCl_3$ leads to a strong single-color violet emission with a maximum PLQY of 96.5%. Furthermore, doping with the trivalent metal halide Ce^{3+} has been investigated, with the goal of improving optical properties, and was found not only to enhance the lattice order by filling the Pb^{2+} and Br^- vacancies, but also to provide additional energy states near the CB, which can facilitate radiative recombination [118,119]. Moreover, H.W. Jang et al. employed BiI_3 as the phase stabilizer and passivation agent to obtain the effective gate-modulated device, showing high hole mobility around 10 $cm^2\ V^{-1}\ s^{-1}$, an on-off current ratio of 10^3, and a low subthreshold swing voltage of 0.43 V dec^{-1} [120]. The most immediate result of doping X-site ions is the tunability of luminescence. R.H. Friend and co-workers controlled the ratio of Cl^- and Br^-, obtaining a sharp, color-pure electroluminescence (EL) from blue to green region of visible spectrum (425–570 nm) [121]. Deschler et al. studied the magneto-optical properties of novel paramagnetic Ruddlesden-Popper hybrid perovskites Mn:$(PEA)_2PbI_4$ (PEA = phenethylammonium) [122], and reported magnetically brightened excitonic luminescence with strong circular polarization from the interaction with isolated Mn^{2+} ions. They found that a dark exciton population is brightened by state mixing with the bright excitons in the presence of a magnetic field, which demonstrated manganese doping as a powerful approach to control excitonic spin physics in Ruddlesden-Popper perovskites.

Another efficient additive is PbI_2. In 2014, Burda et al. studied the perovskite thin fims with different amounts of PbI_2 by transient absorption spectroscopy [123]. The carrier dynamics analysis reveales that perovskite thin films with less PbI_2 exhibit faster relaxation rates compared to those with more PbI_2. These fast kenetics are due to charge carrier trapping, while the slower kinetics in samples containing PbI_2 are due to a passivation effect. Several subsequent papers reported that the addition of PbI_2 in perovskite phase can greatly improve the overall performance of PODs [124–127], because it is able to hinder defects and ion migration, and lead low recombination in PFL (Fig. 8e). The perovskite film is uniform without any pits after adding PbI_2. However, the mechanism of in situ passivation of PbI_2 to improve the efficiency of PODs was not revealed until 2019. Yan et al. systematically investigated the precise PbI_2 ratio and the PbI_2 in situ passivation mechanism based on defect density, carrier lifetime, Fermi level, and so forth [128]. They found that an appropriate ratio of I/Pb is around 2.57:1 using energy-dispersive spectroscopy. And the efficiency of SCs is as high as 19.55% compared to SCs with an I/Pb ratio of 2.69:1 (11.30%).

Similarly, a set of organic compounds or mixed solutions have been used with the aim of eliminating defects and increasing the efficiency of PODs. Zhang's reasearch group chose [*N*-9″-hepta-decanyl-2,7-carbazole-alt-5,5-(4′,7′-di-2-thienyl-2′,1′,3′-benzothiadiaz-ole)] (PCDTBT) as the electron donor polymer in $MAPbI_xCl_{3-x}$ [129], and they believed that PCDTBT would interact with the $MAPbI_xCl_{3-x}$ and form a "Stonehenge-like" structure. The fabricated thin films show more ordered orientated crystallization and a high quality, and the devices also exhibit small hysteresis as well as enhanced stability, which are attributed to the reduction of defects. And as shown in Fig. 8f, Troshin et al. showed that the photothermal aging of perovskites can be significantly suppressed by using

polyvinylcarbazole (PVC) as a stabilizer [130]. Introducing an optimal content of PVC into $MAPbI_3$ delivers a PCE of 18.7% in combination with a significantly improved SC operational lifetime: devices retained ~70% of the initial efficiency after light soaking for 1500 h, whereas the control samples without PVC degraded almost completely under the same conditions. Recently, Liu, Huang and Gao et al. have focused on the ignored hydrogen bonds, which plays a critical role in affecting defect passivation. They obtained high efficient LEDs through rational design of passivation molecules, namely, 2,2′-(ethylenedioxy)diethylamine (EDEA) and hexamethylenediamine (HMDA). They exploited O atoms within the passivation agents (PAs) to polarize the passivating amino groups through the inductive effect, thereby reducing their electron-donating ability and relevant hydrogen-bonding ability. This leads to the enhanced coordination of PA functional groups with perovskite defect sites, which greatly improves the passivation efficiency. As a result, these LEDs are able to significantly reduce the defect-mediated non-radiative recombination and boost the EL performance with an average EQE of $19.0 \pm 0.8\%$ and a record value of 21.6%. Later, Sirringhaus reported a surface cleaning and passivation technique, the cleaning-healing-cleaning (C–H–C) process, utilizing organic polar and non-polar solvents [131]. This approach can reduce the concentration of ionic surface defects in halide-based perovskites without disturbing the crystal lattice. Surface treatment restores clean, near hysteresis-free transistor operation even when the perovskite thin films are formed under non-optimized conditions and can improve room temperature FETs mobility by two to three orders of magnitude compared to untreated films. The fabricated FETs exhibited high *n*- and *p*-type mobilities of 3.0 $cm^2 V^{-1} s^{-1}$ and 1.8 $cm^2 V^{-1} s^{-1}$, respectively, at 300 K, and higher values (9.2 $cm^2 V^{-1} s^{-1}$; *n*-type) at 80 K. More interestingly, this method can be used to transform PbI_2 single crystals into high-quality, two-dimensional perovskite single crystals. Nazeeruddin et al. obtained hysteresis-free perovskite transistors with excellent stability through molecular cross-linking and amine-based surface passivation [132]. They added diethyl-(12-phosphonododecyl)phosphonate to the precursor solution to obtained a smooth and dense perovskite layer composed of tightly bound grains, which significantly suppressed iongeneration and migration. Afterwards, they achieved efficient surface passivation of perovskite films after surface treatment with an amine-bearing polymer, i.e., polyethylenimine ethoxylated. This work demonstrates the first perovskite transistor with complete hysteresis and unprecedented stability in continuous operation under ambient conditions. More importantly, it also achieves bipolar transport with opposite carriers, with equilibrium hole and electron mobilities of 4.02 and 3.35 $cm^2 V^{-1} s^{-1}$, respectively. Recently, a perovskite grain molecular cross-linking approach combined with amine-based surface passivation was introduced to suppress the generation and migration of ions [133]. This approach was achieved through hydrogen bond interactions between perovskite halogens and dangling bonds present at GBs and a hydrophobic cross-linker, namely diethyl-(12-phosphonododecyl)phosphonate, added to the precursor solution. As a consequence, the smooth and compact perovskite layers composed of tightly bound grains were obtained, and

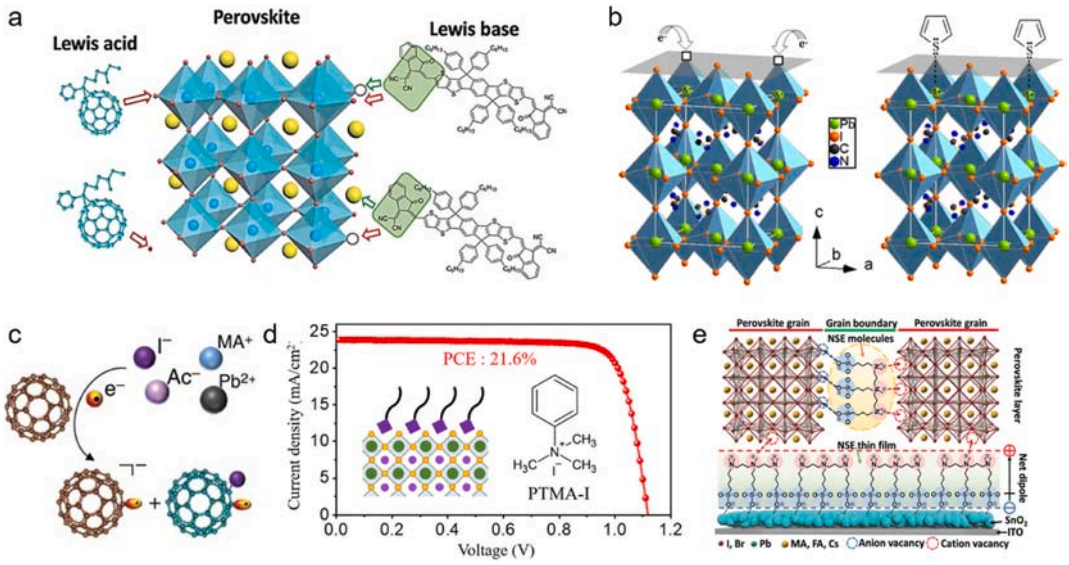

Fig. 9. (a) Schematic reaction process of perovskite growth resulting from the combination of the Lewis base BrPh-ThR in the perovskite-solution precursor and the Lewis acid bis-PCBM in the antisolvent process. Reproduced with permission from Ref. [134]: Copyright 2021, John Wiley and Sons. (b) Possible nature of trap sites and proposed passivation mechanism. Left: Loss of iodine at the surface of the perovskite leads to vacancy sites (hollow boxes) and a resulting net positive charge residing on the Pb atom (shown in green). Photogenerated electrons are then able to fall into this Coulomb trap site, thus neutralizing the charge and rendering the crystal more stable. Right: Thiophene or pyridine molecules can donate electron density to the Pb and form a coordinate or dative covalent bond, effectively neutralizing the excess positive charge in the crystal. Reproduced with permission from Ref. [135]: Copyright 2014, American Chemical Society. (c) A schematic of in-situ passivation of halide-induced DLDS: PCBM adsorbs on Pb–I antistite defective grain boundary during perovskite self-assembly. Reproduced with permission from Ref. [143]: Copyright 2015, Springer Nature. (d) Schematic illustration of quaternary ammonium halides (QAHs) assembled on the defect sites. The red and blue symbols represent the N atom and O atom of the choline chloride molecule, respectively. Reproduced with permission from Ref. [146]: Copyright 2021, American Chemical Society. (e) Schematic illustration of the synergistic effects of MSAPBS to lower the perovskite WF and passivate perovskite lattice defects. Reproduced with permission from Ref. [147]: Copyright 2019, John Wiley and Sons.

the corresponding FET showed ambipolar transport of opposite carriers with balanced hole and electron mobilities of 4.02 and 3.35 $cm^2\ V^{-1}\ s^{-1}$, respectively. Meanwhile, the high I_{on}/I_{off} ratio is as high as 10^4, and the lowest sub-threshold swing of 267 mV dec^{-1} reported to date for any perovskite transistor.

4.3. Lewis acid or base

Due to their ionic nature, a high density of charged point defects may exist in perovskite materials. For example, highly mobile halide anions with low migration activation energy constitute Frenkel-type point defects [75]. These charged defects act as traps to scatter photo-generated charge carriers to hinder charge carrier transport. To compensate for the partial charge, deactivators of Lewis acid and Lewis base were developed (Fig. 9a) [134]. A Lewis acid is a molecule or ion that accepts an electron pair, whereas a Lewis base donates a pair of electrons. A variety of deactivators with Lewis base functional groups have been developed. Snaith et al. introduced Lewis base molecules as N or S donors at perovskite/Spiro-MeOTAD interface for the first time, resulting in a significant increase in PCE from 13% to 15.3% and 16.5% [135]. They proposed that Lewis bases can passivate the under-coordinated Pb ions in perovskite crystals through the coordination bonding between the sulfur atoms in thiophene or nitrogen atoms in pyridine (Fig. 9b). It is found that treatment of metal halide perovskite thin films with pyridine and thiophene can effectively reduce non-radiative recombination and increase PL lifetime from 340.7 to 2234.2 and 2016.5 ns [136]. And the defects densitiy decreases from 3.5×10^{16} to 1.0×10^{16} and 0.2×10^{16} cm^{-3}, respectively. Based on the spatially resolved confocal PL measurement, the enhanced PL lifetime are experimentally correlated with the enhanced PL at the GBs, indicating the passivaition of GBs defects. Meng et al. investigated the effect of Lewis bases on the ripening process of perovskite thin films, and confirmed the interaction between the Lewis base and PbI_2/or perovskites. They claimed that the introduction of Lewis bases can further promote the ripening process and aid in grain growth [137]. In 2015, Park and co-workers fabricated reproducibly high efficiency perovskite SCs via Lewis base adduct of lead (II) iodide [8]. The adduct-induced $CH_3NH_3PbI_3$ exhibits high charge extraction properties with a high hole mobility of 3.9×10^{-3} $cm^2\ V^{-1}\ s^{-1}$ and a slow recombination rate. The average PCE of 41 cells was 18.3% and the best value of 19.7% was obtained by the adduct approach. Apart from perovskites, Lewis bases are often used for passivation at the PODs interfaces. Last year, Haque et al. revealed that chemical binding of charge transport layers to $CH_3NH_3PbI_3$ defect sites is an integral part of the interfacial charge injection mechanism in both n-i-p and p-i-n architectures [138]. The PL and XPS determined that the binding interaction occurs through Lewis base interactions between electron-donating moieties on HTLs and the $CH_3NH_3PbI_3$ surface. Transient absorption measurements show that the yield and lifetime of injected charges are greatly enhanced in those HTLs that undergo strong binding interactions. Meanwhile, dual-Lewis-base molecules were adopted by Tang et al. to modify the interfaces, and pure-red perovskite LEDs were obtained [139]. They employed three structurally similar dual-Lewis-base molecules ethylenediamine, ethanolamine and beta-alanine to modify the interfaces. And the functional groups in these molecules can enhance the hydrophilicity of the HTL surface, thereby improving the quality of perovskite thin films and supressing the formation of unfavorable low-order ($n = 1$ and $n = 2$) phases. The optimal LEDs achieve a pure-red emission at 634 nm with a maximum luminance of 9218 cd m^{-2} and a peak EQE of 5.27%.

Similar to Lewis base, Lewis acid was used to passivate electron-rich defects. Typical passivation agent for negatively charged defects is fullerene (C_{60}) and its derivatives, as shown in Fig. 9c. Lewis acids were used to passivate under-coordinated halides and antisite PbI^{3-}. Huang et al. are the first to demonstrate the passivation of phenyl-C61-butyric acid methyl ester ($PC_{61}BM$) for DLDS and SLDS at GBs and perovskite/C_{60} interface in the inverted SCs [140]. Following this report, many works have been carried out to investigate the effects of fullerene and its derivatives on device performance and hysteresis [141–143]. For example, Xu et al. mixed $PC_{61}BM$ with perovskite solution and observed that $PC_{61}BM$ can passivate Pb–I antisite defects [143]. DFT calculations show that the work function of the ground state is hybridized with the introduction of $PC_{61}BM$, which suggests that $PC_{61}BM$ could passivate iodide-rich defect sites and reduce iodide ion migration under applied electric field, hysteresis and unstable diode behavior. Cho and co-workers chose $PC_{61}BM$ to improve the thermal stability of organometal halide perovskite crystals, which also improved the PCEs of the related SCs [144]. They found that this Lewis acid is located at GBs and reacts with halogens in perovskites to induce electron transfer. The reaction products chemically passivate perovskite crystals and strongly bind halogen atoms at GBs to their crystal lattice, preventing them from exiting from the crystal lattice, thereby improving thermal stability of perovskite crystals. Wang et al. reported an efficient method to prepare high performance n-i-p type planar heterojunction perovskite SCs [145]. The fullerene derivative layer between the ETL and PFL significantly improves electron extraction and suppresses charge recombination by reducing defect density at the interface, further eliminating hysteresis and stabilizing power output over 20% by composition. Furthermore, $PC_{61}BM$ is also a good electron transporting material. Addition of $PC_{61}BM$ on the top of or inside the PFL significantly reduces the defect density and reduces the *J-V* hysteresis caused by trapped charge at the interface or inside the bulk. Similarly, π-conjugated small molecules are also used as charge transport layers, which can passivate defects at the interface with the PFL. However, compared to Lewis bases, the researches on Lewis acids have been more limited. More efforts are required to develop novel Lewis acid molecules to efficiently passivate under-coordinated halide or Pb-X transposition defects for efficient and stable PODs.

Compared with pure positively or negatively charged defects, the probability of coexistence of the two is always higher in PODs, thus requiring the synergistic use of Lewis acids and Lewis bases. On this basis, Cho et al. demonstrated that quaternary ammonium halide additives (Fig. 9e) with positive and negative charges can effectively passivate the positively and negatively charged defects simultaneously [146]. The treated perovskite SCs achieved a certified PCE of 21.6%, due to the significant reduced defect density. And Ma and co-workers introduced onconjugated multi-zwitterionic small-molecule electrolytes (NSEs), passivating charged defects at the perovskite bulk/interfaces via a spontaneous bottom-up passivation effect. Implementing these synergistic properties affords NSE-based planar perovskite SCs that deliver a remarkable power conversion efficiency of 21.18% with a maximum $V_{OC} = 1.19$ V, in combination with suppressed hysteresis and enhanced environmental, thermal, and light-soaking stability [147]. However, a key

limitation of small molecule passivators is that they may not be able to maintain their interaction with perovskites under severe operating conditions such as high temperature or bias [148]. The reason for this is their high diffusivity and weak secondary bonding with perovskite. In this regard, polymer additives with multiple Lewis base and/or acid functional groups may be better candidates to provide long-term and permanent passivation of defects in PODs. In addition, thiourea (TU) can be served as a Lewis acid-base adduct [149]. The crystal grains of the treated perovskite thin films are smooth and large in size, and the best performance of SCs with TU exhibits a PCE of 19.80%, and an average steady-state PCE of 18.60% with potent stability under ambient air. It is noted that the interaction between Lewis acids and Lewis bases can control the morphology of perovskite thin films. Zhu et al. obtained Lewis acid-base interaction-induced porous PbI_2 film by 4-*tert*-butylpyridine (TBP) vapor treatment method [150]. The complete reaction of porous PbI_2 with CH_3NH_3I yields continuous, uniform, and PbI_2-free perovskite film with large grains. As a result, a promising PCE of ~18% is achieved in planar-heterojunction perovskite SCs.

Apart from these, the positive azeotrope solvents may also act as Lewis bases (acids), which enable a reduction in defect density and substantial improvement in performance and stability of *n*-type (*p*-type) PODs. For example, *n*-type $MAPbI_3$ FETs treated by Lewis bases, such as ethyl acetate, methyl acetate, and diethyl ether, all exhibited higher I_{on} than their corresponding pristine ones [115]. Similarly, 1,3,5-tribromobenzene-treated $FAMAPbBr_3$ FETs showed enhanced performance (*p*-type) compared to the pristine ones. Although the solvent-based Lewis acid/base treatments worked well for top-gate bottom-contact devices, they failed to have any effect on the performance of bottom-gate bottom-contact devices, probably because the solvent effect is mainly limited to the surface of perovskite films.

4.4. Transport materials

Rationally utilization of ETL/HTL may be one of the effective ways to the high performance promote PODs, because defect states exist not only in perovskites or interfaces, but also in the charge transport layers themselves. The properties of these charge transport layers have a significant impact on the optoelectronic properties of PODs, and in the past few years, many new charge transport layers have been reported. One of the most commonly used ETL materials is TiO_2, which enables efficient electron injection and hole blocking. The TiO_2 used in PODs can be in a dense form or a mesoporous structure. However, it has been reported that Ti^{3+} acts as the main surface defects in dense TiO_2, so the deposition of perovskite crystals on TiO_2 may lead to the formation of defect states [151, 152]. Furthermore, mesoporous TiO_2 is extremely unstable under ultraviolet irradiation [153]. Currently, various interface engineering strategies have been developed to alleviate this situation. For example, Hayase et al. inserted a HOCO-R-NH^{3+}I interlayer between mesoporous TiO_2 and PFL to pacify the surface defect states [154]. Fullerene self-assembled monolayers (C_{60}-SAM) have also been successfully used to suppress non-radiative recombination with the added benefit of reducing *J-V* hysteresis [155]. Steiner et al. found that doping TiO_2 with Al^{3+} can eliminate oxygen defects and imporove the performance and stability of PODs [156]. This enhancement can be attributed to the substitutional incorporation of Al in the anatase lattice, which "permanently" passivates electron defect sites in the bulk and at the surface of TiO_2.

Besides the modification method, TiO_2 is also replaced by other metal oxides, such as ZnO [157] and SnO_2 [158]. Zheng et al. passivated the surface of ZnO with thin layers of MgO and protonated ethanolamine (EA), achieving an optimal efficiency as high as 21.1% without hysteresis. When further encapsulated with graphene, the performance was mantained in air for over 300 h [157]. In another example, You et al. were able to improve the surface properties of ZnO by adding hydrophilic and insulating polymer (polyvinyl pyrrolidine, PVP) to modify its surface properties and reduce non-radiative recombination, thereby increasing the EL efficiency (around 10.43 ph el$\%^{-1}$) [159]. However, due to the poor chemical compatibility between ZnO and organo-metal halide perovskites, PODs must be coated with other materials. This increases the complexity of the preparation, so SnO_2 needs to be considered for replacement. SnO_2 has a wider bandgap of 3.8 eV and higher electron mobility than ZnO [158]. Importantly, SnO_2 has better stability in ambient air without encapsulation. The related SCs achieved PCE and V_{OC} above 18% and 1.19 V. Organic conjugated small molecules are also used to facilitate electron transport. Park et al. used an electron transporting small molecule organic material (TPBI) dissolved in a nonpolar volatile solvent to reduce perovskite crystal grain size and to improve electron injection into PFL during perovskite crystallization [160]. Moreover, the organic small molecules exhibit a graded distribution along the film thickness, enhancing ETL for better charge balance in PODs, resulting in improved luminance and EL efficiency (around 8.79%).

Compared to materials that can be used as ETLs, the HTLs are more selective. In PODs, due to the relatively deep VBM of metal halide perovskites, there is a large energetic hole injection barrier between the anode and PFL. Therefore, an interfacial buffer layer with an intermediate ionization potential must be used between the anode and the PFL. Various solution-processable hole-transporting conjugated polymer materials with appropriate highest occupied molecular orbital (HOMO) energy levels to bridge the anode and PFL are suitable, such as poly(*N*-vinylcarbazole), poly[*N,N*′-bis(4-butylphenyl)-*N,N*′-bis(phenyl)-benzidine](poly-TPD) [161], and poly(9, 9′-dioctylfluorene) [162]. Rand and co-workers showed that the addition of long-chain ammonium halides to the precursor solution can significantly hinder the grain growth of 3D perovskite crystallites and reduce film roughness [161]. Moreover, long-chain ammonium cations stabilize the grain surface, resulting in an enhanced PL and EL emission, as well as operational stability. They claimed that the incorporation of long-chain ammonium halide ligands into perovskite thin films may benefit other devices such as FETs, SCs and lasers. Wang et al. developed PCDTBT and PCDTBT1 as new HTLs [163]. The result shows that these conjugated polymers can help eliminate a certain number of defects due to the synergistic passivation of thiophene and methoxy units. Furthermore, devices using PCDTBT and PCDTBT1 as HTL exhibited remarkable stability and maintained 90% of PCE for more than 30 days under humid conditions due to their hydrophobicity. Recently, several groups have attempted to replace organic HTLs with inorganic materials. Using copper phthalocyanine (CuPc) nanorods as the HTL, the defects on the surface of perovskite thin films were supressed [164]. Compare with traditional HTLs, CuPc has low cost and highly stable. The final PCE of the passivated device kept at

14.7% measured under one sun illumination for 600 h. In contrast, the PCE of the conventional device dropped by 92%.

It should be noticed that PODs may exhibit serious self-degradation phenomenon when Au, Ag or Al is selected as electrodes [165–167]. This is caused by intrinsic ionic defects in the PFL as well as the presence of Au–I bonds on the electrode surface, as shown in Fig. 10a. To suppress the ionic defects and Ag–I bonds, Back et al. introduced an amine-mediated titanium suboxide (AM-TiO_x) as a chemical inhibition layer (CIL) [166]. Compared to PODs without CIL, the device performance maintained nearly 80% of its initial PCEs even after 1 year (9000 h) storage under nitrogen conditions.

It is worth mentioning that Snaith and co-workers designed a sandwich-structure within a cavity composed of a thin-film (~7 μm) cholesteric liquid crystal (CLC) reflector and a metal back-reflector [168]. The threshold fluence (~7 μJ cm^{-2}) for ASE in the perovskite film is reduced by at least two orders of magnitude in the presence of the CLC reflector, which can be due to the improved coupling of the oblique and out-of-plane modes that are reflected into the bulk in addition to any contributions from cavity modes. The work suggests a promising route to single-mode "mirror-less" lasing from perovskite materials with the CLC providing additional potential functionality, such as flexible substrates and allowing wavelength-tunability, in addition to acting as the reflector. Flexible lasers may find use in flexible displays or military applications such as friend or foe identification.

4.5. Multi-dimensional perovskite materials

Compared with 2D perovskites, 3D perovksites exhibit severe degradation under humid conditions. However, the performance of the former is not good as the latter [169]. Therefore, a novel approach which combines the advantages of these different dimensions of perovskites was proposed. The advantages of this approach can be mainly attributed to the following three aspects. First, when the 2D perovskite is incorporated into the 3D perovskite surface, the vacancies are effectively filled and interacted with under-coordinated Pb atoms, significantly improving the quality of perovskite crystals. Then, 2D perovskites act as a robust barrier on the 3D perovskites to prevent moisture/oxygen erosion and inhibit ion migration, thereby inducing hydrophobicity and large formation energy for enhanced stability. Finally, the heterostructure induced by the stacking of 2D/3D perovskites provides different energy levels for carriers transport. Higher and lower energy levels were obtained in the 2D and 3D counterparts, respectively, effectively facilitating charge transfer/extraction, thereby enhancing the performance of the PODs.

Due to the similarity in lattice constants between 2D and 3D perovskites, Grancini et al. fabricated this 2D/3D (HOOC$(CH_2)_4NH_3)_2PbI_4$/$CH_3NH_3PbI_3$ perovskite heterostructure and demonstrated that this structure contributes to significantly improve

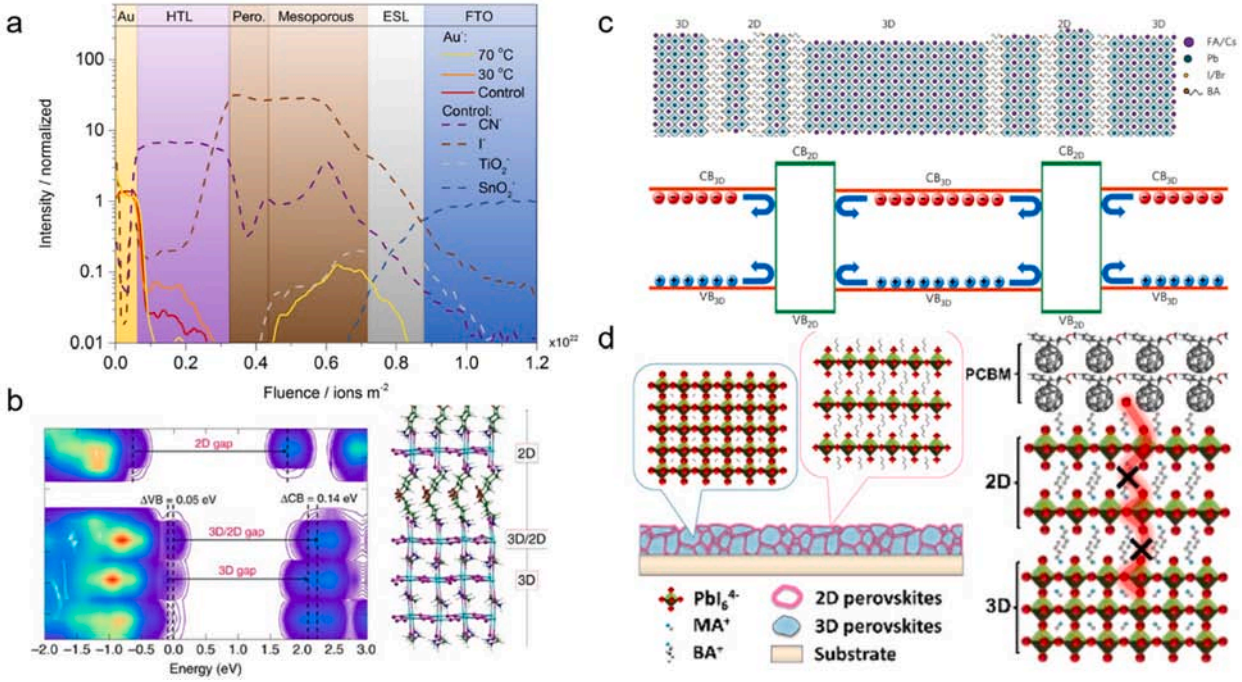

Fig. 10. (a) Profile showing the concentration of selected species across the control device. The profile of Au^- is compared to that of the devices aged at 30 and 70 °C. Reproduced with permission from Ref. [165]: Copyright 2016, American Chemical Society. (b) Local density of state (DOS) of the 3D/2D interface and interface structure with the 2D phase contacting the TiO_2 surface. Reproduced with permission from Ref. [170]: Copyright 2017, Springer Nature. (c) Illustration of the proposed self-assembled 2D-3D perovskite film structure and electronic band offsets of the 2D-3D heterojunction. (d) Proposed electronic band offsets of the 2D-3D heterojunction. CB and VB stand for conduction band and valence band, respectively, with the subscript indicating either the 2D or 3D phase (bottom). Reproduced with permission from Ref. [173]: Copyright 2017, Springer Nature. (e) Degradation mechanism in the schematic diagram of the formation of 2D/3D stacked structures in A-treated perovskite films. Reproduced with permission from Ref. [174]: Copyright 2018, American Chemical Society.

the stability of PODs over one year, reaching the highest recorded value [170]. Xing et al. introduced hydrophobic 3-(trifluoromethyl) phenethylamine hydroiodide (CF_3PEAI) on the surface of perovskite films. CF_3PEAI can form 2D perovskites that penetrate deep into the thin films (>30 nm) to further passivate internal defect states and improve the long-term stability. This perovskite SCs retained 98% of their initial performance after 528 h in ambient air with a humidity of 70–80%. First-principle simulations revealed that CF_3PEAI effectively renormalizes vacancy defect states with benign characteristics, improving the performance from 18.87% to 21.05%. Similarly, Zeng et al. developed a facile energy cascade channel strategy to fabricate self-organized and controllable 2D/3D perovskites by introducing guanidine hydrobromide (GABr), which greatly increases the efficiency of blue perovskite LEDs [171]. The 2D/3D perovskites structure enhances the energy cascade, supresses free charge diffusion, and enhances radiative recombination. Benefiting from this energy cascade channel, the EQE of blue perovskite LEDs emitting at 492 nm is significantly improved from 1.5% to 8.2%. A more interesting study was conducted by Wolf et al. on the dimensionality (n) of 2D perovskite fragments at the electron-selective interface of inverted perovskite SCs [172]. They obtained damp heat-stable pervoskite SCs by tuning the dimensional fragments of the 2D perovskite layers. These fragments are formed with oleylammonium-iodide molecules at room temperature, which passivate the perovskite surface at the electron-selective contacts. The resulting inverted perovskite SCs deliver a PCE of 24.3% and retain >95% of their initial value after >1000 h at damp-heat test conditions. In addition, 2D perovskite passivation affects the surface morphology, including grain size and roughness. Wang et al. introduced BA into 3D perovskite to fabricate $BA_x(FA_{0.83}Cs_{0.17})_{1-x}Pb(I_{0.6}Br_{0.4})_3$ perovskite SCs and found that the 2D phase was helpful to improve the crystallinity of the perovskite thin films (Fig. 10c) [173]. The 2D perovskite plates form above the 3D grains and are brighter than the adjacent grains, which is ascribed to the charge accumulation because 2D perovskite has a lower conductivity. The champion device has a PCE of 20.6%. More importantly, the 2D/3D perovskites have excellent stability. And in Fig. 10d, the degradation mechanism was proposed in 2D/3D stacking and 3D devices. The 2D/3D stacking perovskite SCs fabricated by two different post-processing methods were both demonstrated to effectively improve device performance through passivation and self-healing effects [174]. Bolink and co-workers reported a 2D/3D/2D perovskite heterostructure by a dual-source vacuum deposition technique [175]. The 2D/3D/2D heterostructure topography exhibited a smaller $R_{RMS} = 8$ nm and a reduced z_{AVG} of 27 nm. Furthermore, the height distribution in the passivated film tends to be narrower, suggesting a more uniform surface after the deposition of 2D perovskite.

All in all, the 2D/3D heterostructured perovskites not only widen the bandgap of 3D perovskites, but also help to reduce the defect density. In addition, the introduction of 2D perovskites into 3D perovskites shows great promise in the preparation of gradient perovskite films.

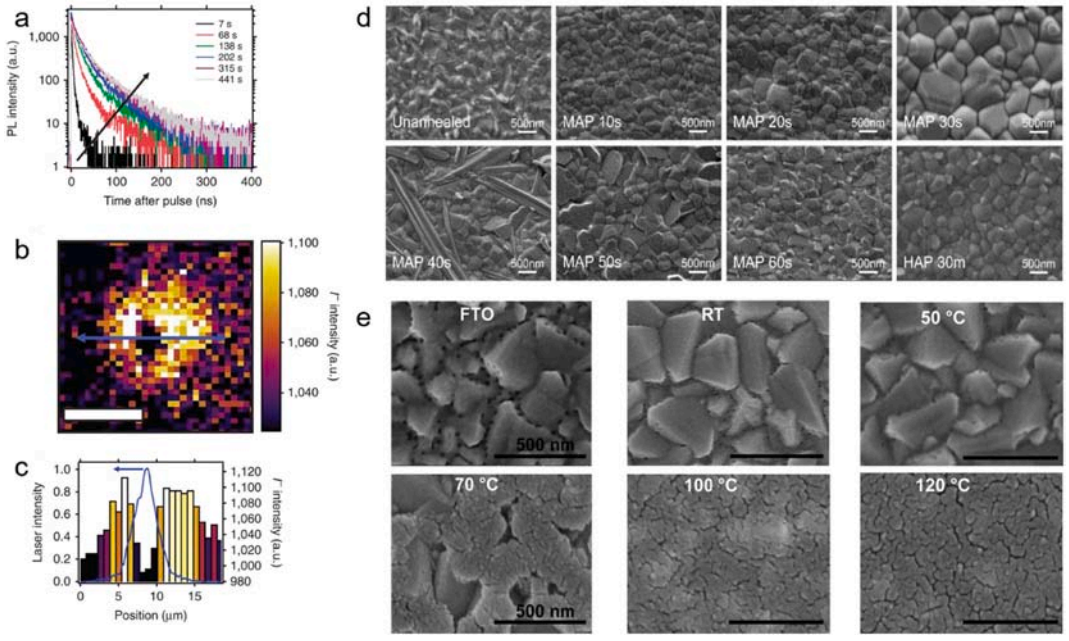

Fig. 11. (a) A series of time-resolved PL decays from a $CH_3NH_3PbI_3$ film measured over time under illumination before time-of-flight secondary-ion-mass spectrometry (ToF-SIMS) measurements. The sample was photoexcited with pulsed excitation (470 nm, 1.2 kJ cm^{-2}). (b) ToF-SIMS image of the iodide (I^-) distribution summed through the film depth (the image has been adjusted to show maximum contrast), scale bar, 10 μm. (c) Line scan of the blue arrow in b to show the iodide distribution (right axis). The measured spatial profile of the illumination laser (blue) is shown on the left axis. Reproduced with permission from Ref. [178]: Copyright 2016, Springer Nature. (d) Top-view SEM image of the microwave-annealing-process perovskite film with different annealing cycles of 10–60 s, using optimal 30 min hotplate-annealing-process perovskite as reference. Reproduced with permission from Ref. [186]: Copyright 2019, John Wiley and Sons. (e) SEM images of (a) bare FTO substrate and NiO thin films prepared on FTO substrates using different substrate temperatures of room temperature, 50 °C, 70 °C, 100 °C and 120 °C. Reproduced with permission from Ref. [193]: Copyright 2019, Elsevier.

4.6. Physical passivation methods

The above-mentioned methods of passivating defects can be classified as chemical methods because a large number of chemical reactions are involved in the fabrication processes. The reduction of defects is closely related to the composition of perovskites, the properties of the dopants/passivation layers, and the device configuration. However, in addition to chemical methods, some more direct methods have recently been developed to reduce the inherent defects in perovskite thin films. Although relatively speaking, most of them have been shown to be very effective in improving the efficiency and stability of PODs.

4.6.1. Light

Due to the particularity of perovskite structure, light-induced transformation is very common. Generally, light has a dual effect on defects. On the one hand, it will lead to the formation of defects [176]. On the other hand, it can repair defects under certain conditions [177]. For example, Stranks et al. found that the PL lifetime and PL intensity increase substantially in $MAPbI_3$ over time under illumination, corresponding to nearly an order-of-magnitude reduction in defect densities (Fig. 11a) [178]. Angelis et al. employed a first principle computational modeling of defect migration under light irradiation, and demonstrated that light promotes the annihilation of iodine vacancy/interstitial Frenkel pairs [179]. Recently, a new behavior in hybrid perovskite has been proposed that can passivate local distortions under light illumination. Mohite and co-workers found that $FA_{0.7}MA_{0.25}Cs_{0.05}PbI_3$ hybrid perovskite thin films undergo uniform lattice expansion under continuous light illumination [180]. After passivation by light, the PCE increased from 18.5 to 20.5% with improved stability. The use of light to passivate PODs made a huge breakthrough in 2019. Sadrameli et al. reported a novel, facile, fast and low cost method for the recovery of degraded PODs based on UV irradiation [181]. They proposed that the passivation of SLDS and DLDS occurs through the dissociation of adsorbed hydroxyl groups and water molecules, respectively. And this method not only fully restores the performance of the aged devices, but also achieves an increase in its efficiency. In our recent study, ASE from core-shell perovskite nanocrystals was observed after exposure to a pulsed nanosecond laser of 355 nm for a period of time, demonstrating the effectiveness of UV irradiation for defect passivation [182]. Moreover, the ultra-low threshold of 447 nJ cm^{-2} provided new perspectives for the design of pervoskite lasers. In addition, the secondary crystallization caused by laser irradiation has been observed [183], suppressing the nonradiative recombination channels, including low defect density, reduced Auger recombination, and weak exction-phonon interaction. Benefiting from these, a low ASE threshould of 5.6 μJ cm^{-2} and high gain value of 743 cm^{-1} were achieved. And in 2021, Stranks et al. examined the sensitivity of this light effect to various experimental considerations to resolve these seemingly conflicting literature reports [184].

4.6.2. Microwave

Recently, a rapid microwave annealing process that replaced the traditional hotplate annealing process is reported to reduce the processing time of perovskite to less than 1 min. Liu et al. used the microwave irradiation to treat perovskite thin films through a one-step deposition method for several minutes at a fixed output power [185]. Duo to the less energy loss and time consumption, the photovoltaic performance of the corresponding SCs is enhanced. Qin and Huang et al. used this method to realize planar heterojunction perovskite SCs [186], as shown in Fig. 11d. These perovskite thin films exhibit a pure crystalline phase, long charge carrier lifetime, and low defect density, which can substantially improve the PODs efficiency without additional enhancer/passivation layer. In the same year, monoclinic phase perovskites were synthesized using microwaves irradiation [187], which exhibited electrochemically switchable electrochemiluminescence. In addition to the effective treatment of perovskite layers, microwaves can also realize the regulation of ETL/HTL. Gao et al. demonstrated efficient PODs for ultrafast synthesis of SnO_2-QDs under conventional microwave assistance [188]. The performance of perovskite SCs based on $CH_3NH_3PbI_3$ increased from 19.77% to 20.24% with higher V_{OC}.

4.6.3. Processing technique

In the process of preparing perovskite thin films, appropriate method can be selected to reduce the defect density and control the surface morphology. Among the most commonly used solution preparation methods, the two-step method can improve uniformity and reduce defect density [189]. Moreover, vacuum-flash assisted solution processing (VASP) has been reported to improve crystal quality. Li et al. removed most of residual solvent, resulting in improved crystallization of the perovskite intermediate phase [190]. Meanwhile, the devices fabricated by the VASP method have better stability and photodegradation resistance. Based on this method, they were able to fabricate SCs with an aperture area exceeding 1 square centimeter, a maximum efficiency of 20.5%, and a certified PCE of 19.6%. In addition, atomic layer deposition (ALD) is another efficient method to passivate interfacial defects. The ALD-Al_2O_3 monolayers will facilitate the separation of photogenerated carriers and improve the performance of PODs due to the suppression of vacancies [191]. The average PCE was increased from 10.33% to 15.06%, and the efficiency achieved was as high as 16.08%. They also suggested that the passivation of defects using the ALO of monolayers might provide new pathway for the improvement of all types of PODs. Increasing crystal grain size and reducing the surface roughness are of great significance for the reduction of defects. Mohite and co-workers reported a hot-casting technique to synthesize large-scale crystalline perovskites with fewer defects, and improved device performance [192]. This technique can obtain large grains in perovskites, which help to reduce GBs and significantly increase the probability of carriers recombination. In addition, Namkoong and co-workers developed a new hot-casting technique, and fabricated densely-packed, less defective NiO films successfully, as shown in Fig. 11e. When the hot-casting temperature was 120 °C, the thin film exhibited an ordered chemistry with strong Ni–O octahedral bonding and facilitated charge extraction at NiO/perovskite interface, resulting in a negligible hysteresis and light soaking.

5. Summary and outlook

Duo to their excellent properties, perovskites may have the potential to change current prospects in the field of optoelectronic devices. Although the efficiency of various devices has greatly improved over the past few years, there is still a long way to go for PODs to be fully commercialized on a large scale. Urgent issues need to be addressed, such as poor stability and ambiguous working mechanisms. Most importantly, all of these thorny problems are related to the defects based on current understanding of perovskite materials and devices, including bulk defect states in perovskite and the interfaces defect states in PODs. Therefore, defect engineering is essential. Surface ligands and defect-passivation molecules on polycrystalline thin films have been demonstrated to be important for improving the electrical properties of metal halide perovskites, which directly translates into improved the efficiency of PODs, material storage lifetime, device lifetime, and processability. Therefore, achieving efficient ligand and surface engineering will be a critical step to overcome current technological limitations and achieve high efficiency and long-term stability for applications.

Compared with conventional materials, metal halide perovskites possess relatively low binding energies and long diffusion lengths, so the perovskite/charge transport layers interfaces must be developed in a way that emphasizes preventing unwanted loss of charge carriers and excitons. Additionally, the surface of the perovskites and interfacial layers should be modified to minimize the number of interfacial defects and nonradiative recombination paths.

Furthermore, ions in perovskites are known to drift under electric fields due to the existence of GBs and ionic vacancies. Therefore, ion migration can be mitigated by a variety of approaches, including improving the microstructure of perovskite thin films, reducing GBs, using cations with less polarity and less directional mobility, or in *n*-type (*p*-type) perovskites Lewis base (acid) to reduce defect density, *etc*. However, it is still not fully understood how ion migration affects the performance of PODs, how ions move, and how ion migration is fundamentally inhibited. In particular, understanding the unique ionic properties of MHPs will be very helpful in effectively mitigating ion transport and even using it for ion-involved optoelectronics, such as artificial synapses.

Efficiency concerns have now alleviated, however, lead stability and toxicity remain challenges. In the long term, there is a preference for environmentally friendly materials to replace lead halide perovskites with materials of comparable performance. Much has been done on the optoelectronic properties of lead-free perovskites, but their efficiency is currently far from that of lead-based perovskites [194,195]. Currently, studies on lead-free perovskites have shown that simply replacing lead with other metal cations in new perovskites often leads to a drop in device efficiency. Some of the modulation methods in this paper may yield unexpected results in improving the efficiency of lead-free perovskite devices.

Fully understanding the nature and causes of defect states in perovskites is a tedious task, and identifying their effects and developing principles for mitigating them are critical to reducing PODs losses. So far, a combination of theoretical and experimental methods has proven to be very effective in uncovering major problems. This ultimately determines the efficiency of various PODs in recent years and is likely to continue to play an important role in the future. It remains to be seen whether these strategies used in metal halide perovskite devices can also yield effective results in other devices based on lead-free perovskites.

Acknowledgements

This work is supported by the National Natural Science Foundation of China (62174079), Science, Technology and Innovation Commission of Shenzhen Municipality (Projects Nos. JCYJ20220530113015035, JCYJ20210324120204011 and KQTD20150717103136556).

References

[1] J.H. Noh, S.H. Im, J.H. Heo, T.N. Mandal, S. II Seok, Chemical management for colorful, efficient, and stable inorganic-organic hybrid nanostructured solar cells, Nano Lett. 13 (2013) 1764–1769.
[2] Z. Xiao, Q. Dong, C. Bi, Y. Shao, Y. Yuan, J. Huang, Solvent annealing of perovskite-induced crystal growth for photovoltaic-device efficiency enhancement, Adv. Mater. 26 (2014) 6503–6509.
[3] S.D. Stranks, G.E. Eperon, G. Grancini, C. Menelaou, M.J.P. Alcocer, T. Leijtens, L.M. Herz, A. Petrozza, H.J. Snaith, Electron-hole diffusion lengths exceeding 1 micrometer in an organometal trihalide perovskite absorber, Science 342 (2013) 341–344.
[4] H. Oga, A. Saeki, Y. Ogomi, S. Hayase, S. Seki, Improved understanding of the electronic and energetic landscapes of perovskite solar cells: high local charge carrier mobility, reduced recombination, and extremely shallow traps, J. Am. Chem. Soc. 136 (2014) 13818–13825.
[5] C. Wehrenfennig, G.E. Eperon, M.B. Johnston, H.J. Snaith, L.M. Herz, High charge carrier mobilities and lifetimes in organolead trihalide perovskites, Adv. Mater. 26 (2014) 1584–1589.
[6] W.S. Yang, B.-W. Park, E.H. Jung, N.J. Jeon, Y.C. Kim, D.U. Lee, S.S. Shin, J. Seo, E.K. Kim, J.H. Noh, S. II Seok, Iodide management in formamidinium-lead-halide-based perovskite layers for efficient solar cells, Science 356 (2017) 1376–1379.
[7] J.-W. Lee, H.-S. Kim, N.-G. Park, Lewis acid-base adduct approach for high efficiency perovskite solar cells, Acc. Chem. Res. 49 (2016) 311–319.
[8] N. Ahn, D.-Y. Son, I.-H. Jang, S.M. Kang, M. Choi, N.-G. Park, Highly reproducible perovskite solar cells with average efficiency of 18.3% and best efficiency of 19.7% fabricated via Lewis base adduct of lead (II) iodide, J. Am. Chem. Soc. 137 (2015) 8696–8699.
[9] L. Meng, E.-P. Yao, Z. Hong, H. Chen, P. Sun, Z. Yang, G. Li, Y. Yang, Pure formamidinium-based perovskite light-emitting diodes with high efficiency and low driving voltage, Adv. Mater. 29 (2017), 1603826.
[10] M. Yuan, L.N. Quan, R. Comin, G. Walters, R. Sabatini, O. Voznyy, S. Hoogland, Y. Zhao, E.M. Beauregard, P. Kanjanaboos, Z. Lu, D.H. Kim, E.H. Sargent, Perovskite energy funnels for efficient light-emitting diodes, Nat. Nanotechnol. 11 (2016) 872–877.
[11] A. Perumal, S. Shendre, M. Li, Y.K.E. Tay, V.K. Sharma, S. Chen, Z. Wei, Q. Liu, Y. Gao, P.J.S. Buenconsejo, S.T. Tan, C.L. Gan, Q. Xiong, T.C. Sum, H.V. Demir, High brightness formamidinium lead bromide perovskite nanocrystal light emitting devices, Sci. Rep. 6 (2016) 1–10.
[12] X.Y. Chin, D. Cortecchia, J. Yin, A. Bruno, C. Soci, Lead iodide perovskite light-emitting field-effect transistor, Nat. Commun. 6 (2015) 1–9.
[13] B.R. Sutherland, E.H. Sargent, Perovskite photonic sources, Nat. Photonics 10 (2016) 295–302.
[14] Y.-H. Kim, S. Kim, A. Kakekhani, J. Park, J. Park, Y.-H. Lee, H. Xu, S. Nagane, R.B. Wexler, D.-H. Kim, S.H. Jo, L. Martínez-Sarti, P. Tan, A. Sadhanala, G.-S. Park, Y.-W. Kim, B. Hu, H.J. Bolink, S. Yoo, R.H. Friend, A.M. Rappe, T.-W. Lee, Comprehensive defect suppression in perovskite nanocrystals for high-efficiency light-emitting diodes, Nat. Photonics 15 (2021) 148–155.

[15] A. Al-Ashouri, E. Köhnen, B. Li, A. Magomedov, H. Hempel, P. Caprioglio, J.A. Márquez, A.B.M. Vilches, E. Kasparaviciusjoel, J.A. Smith, N. Phung, D. Menzel, M. Grischek, L. Kegelmann, D. Skroblin, C. Gollwitzer, T. Malinauskas, M. Jošt, G. Matič, B. Rech, R. Schlatmann, M. Topič, L. Korte, A. Abate, B. Stannowski, D. Neher, M. Stolterfoht, T. Unold, V. Getautis, S. Albrechet, Monolithic perovskite/silicon tandem solar cell with > 29% efficiency by enhanced hole extraction, Science 370 (2020) 1300–1309.

[16] K. Yoshikawa, H. Kawasaki, W. Yoshida, T. Irie, K. Konishi, K. Nakano, T. Uto, D. Adachi, M. Kanematsu, H. Uzu, K. Yamamoto, Silicon heterojunction solar cell with interdigitated back contacts for a photoconversion efficiency over 26, Nat. Energy 2 (2017) 1–8.

[17] G.J. Bauhuis, P. Mulder, E.J. Haverkamp, J.C.C.M. Huijben, J.J. Schermer, 26.1% thin-film GaAs solar cell using epitaxial lift-off, Sol. Energy Mater. Sol. Cells 93 (2009) 1488–1491.

[18] M. Kaelin, D. Rudmann, A. Tiwari, Low cost processing of CIGS thin film solar cells, Sol. Energy 77 (2004) 749–756.

[19] S.-F. Wu, S.-H. Li, Y.-K. Wang, C.-C. Huang, Q. Sun, J.-J. Liang, L.-S. Liao, M.-K. Fung, White organic LED with a luminous efficacy exceeding 100 lm W^{-1} without light out-coupling enhancement techniques, Adv. Funct. Mater. 27 (2017), 1701314.

[20] J.L. Knutson, J.D. Martin, D.B. Mitzi, Tuning the band gap in hybrid tin iodide perovskite semiconductors using structural templating, Inorg. Chem. 44 (2005) 4699–4705.

[21] G.E. Eperon, S.D. Stranks, C. Menelaou, M.B. Johnston, L.M. Herz, H.J. Snaith, Formamidinium lead trihalide: a broadly tunable perovskite for efficient planar heterojunction solar cells, Energy Environ. Sci. 7 (2014) 982–988.

[22] C.-H. Lu, G.V. Biesold-McGee, Y. Liu, Z. Kang, Z. Lin, Doping and ion substitution in colloidal metal halide perovskite nanocrystals, Chem. Soc. Rev. 49 (2020) 4953–5007.

[23] T.J. Jacobsson, J.-P. Correa-Baena, M. Pazoki, M. Saliba, K. Schenk, M. Grätzel, A. Hagfeldt, Exploration of the compositional space for mixed lead halogen perovskites for high efficiency solar cells, Energy Environ. Sci. 9 (2016) 1706–1724.

[24] M.I.H. Ansari, A. Qurashi, M.K. Nazeeruddin, Frontiers, opportunities, and challenges in perovskite solar cells: a critical review, J. Photochem. Photobiol. C Photochem. Rev. 35 (2018) 1–24.

[25] V.M. Goldschmidt, Die gesetze der krystallochemie, Naturwissenschaften 14 (1926) 477–485.

[26] Q. Sun, W.-J. Yin, Thermodynamic stability trend of cubic perovskites, J. Am. Chem. Soc. 139 (2017) 14905–14908.

[27] Q. Chen, N. Marco, Y. Yang, T.-B. Song, C.-C. Chen, H. Zhao, Z. Hong, H. Zhou, Y. Yang, Under the spotlight: the organic-inorganic hybrid halide perovskite for optoelectronic applications, Nano Today 10 (2015) 355–396.

[28] H.-S. Kim, C.-R. Lee, J.-H. Im, K.-B. Lee, T. Moehl, A. Marchioro, S.-J. Moon, R. Humphry-Baker, J.-H. Yum, J.E. Moser, M. Grätzel, N.-G. Park, Lead iodide perovskite sensitized all-solid-state submicron thin film mesoscopic solar cell with efficiency exceeding 9, Sci. Rep. 2 (2012) 1–7.

[29] J.M. Ball, M.M. Lee, A. Hey, H.J. Snaith, Low-temperature processed meso-superstructured to thin-film perovskite solar cells, Energy Environ. Sci. 6 (2013) 1739–1743.

[30] Q. Dong, Y. Fang, Y. Shao, P. Mulligan, J. Qiu, L. Cao, J. Huang, Electron-hole diffusion lengths > 175 μm in solution-grown $CH_3NH_3PbI_3$ single crystals, Science 347 (2015) 967–970.

[31] J. Burschka, N. Pellet, S.-J. Moon, R. Humphry-Baker, P. Gao, M.K. Nazeeruddin, M. Grätzel, Sequential deposition as a route to high-performance perovskite-sensitized solar cells, Nature 499 (2013) 316–319.

[32] I. Mesquita, L. Andrade, A. Mendes, Perovskite solar cells: materials, configurations and stability, Renew. Sustain. Energy Rev. 82 (2018) 2471–2489.

[33] B. Li, V. Ferguson, S.R.P. Silva, W. Zhang, Defect engineering toward highly efficient and stable perovskite solar cells, Adv. Mater. Interfac. 5 (2018), 1800326.

[34] B. Che, P.N. Rudd, S. Yang, Y. Yuan, J. Huang, Imperfections and their passivation in halide perovskite solar cells, Chem. Soc. Rev. 48 (2019) 3842–3867.

[35] E.J. Juarez-Perez, L.K. Ono, M. Maeda, Y. Jiang, Z. Hawash, Y. Qi, Photodecomposition and thermal decomposition in methylammonium halide lead perovskites and inferred design principles to increase photovoltaic device stability, J. Mater. Chem. 6 (2018) 9604–9612.

[36] Mi-C. Jung, Y.M. Lee, H.-K. Lee, J. Park, S.R. Raga, L.K. Ono, S. Wang, M.R. Leyden, B.D. Yu, S. Hong, Y. Qi, The presence of CH_3NH_2 neutral species in organometal halide perovskite films, Appl. Phys. Lett. 108 (2016), 073901.

[37] B. Conings, J. Drijkoningen, N. Gauquelin, A. Babayigit, J. D'Haen, L. D'Olieslaeger, A. Ethirajan, J. Verbeeck, J. Manca, E. Mosconi, F. De Angelis, H.-G. Boyen, Intrinsic thermal instability of methylammonium lead trihalide perovskite, Adv. Energy Mater. 5 (2015), 1500477.

[38] C. Zhang, T. Andersson, S. Svensson, O. Björneholm, M. Tchaplyguine, Core-shell structure in self-assembled lead/lead-oxide nanoclusters revealed by photoelectron spectroscopy, Phys. Rev. B 87 (2013), 035402.

[39] T.W. Kim, S. Uchida, T. Matsushita, L. Cojocaru, R. Jono, K. Kimura, D. Matsubara, Manabu Shirai, K. Ito, H. Matsumoto, T. Kondo, H. Segawa, Self-organized superlattice and phase coexistence inside thin film organometal halide perovskite, Adv. Mater. 30 (2018), 1705230.

[40] I.M. Hermes, S.A. Bretschneider, V.W. Bergmann, D. Li, A. Klasen, J. Mars, W. Tremel, F. Laquai, H.-J. Butt, M. Mezger, R. Berger, B.J. Rodriguez, S.A.L. Weber, Ferroelastic fingerprints in methylammonium lead iodide perovskite, J. Phys. Chem. C 120 (2016) 5724–5731.

[41] M.U. Rothmann, W. Li, Y. Zhu, U. Bach, L. Spiccia, J. Etheridge, Y.-B. Cheng, Direct observation of intrinsic twin domains in tetragonal $CH_3NH_3PbI_3$, Nat. Commun. 8 (2017), 14547.

[42] M.V. Kovalenko, L. Protesescu, M.I. Bodnarchuk, Properties and potential optoelectronic applications of lead halide perovskite nanocrystals, Science 358 (2017) 745–750.

[43] K.P. McKenna, Electronic properties of {111} twin boundaries in a mixed-ion lead halide perovskite solar absorber, ACS Energy Lett. 3 (2018) 2663–2668.

[44] W.-J. Yin, T. Shi, Y. Yan, Unusual defect physics in $CH_3NH_3PbI_3$ perovskite solar cell absorber, Appl. Phys. Lett. 104 (2014), 063903.

[45] H. Jin, E. Debroye, M. Keshavarz, I.G. Scheblykin, M.B.J. Roeffaers, J. Hofkens, J.A. Steele, It's a trap! on the nature of localised states and charge trapping in lead halide perovskites, Mater. Horiz. 7 (2020) 397–410.

[46] M.-H. Du, Density functional calculations of native defects in $CH_3NH_3PbI_3$: effects of spin-orbit coupling and self-interaction error, J. Phys. Chem. Lett. 6 (2015) 1461–1466.

[47] D. Meggiolaro, E. Mosconi, F. Angelis, Mechanism of reversible trap passivation by molecular oxygen in lead-halide perovskites, ACS Energy Lett. 2 (2017) 2794–2798.

[48] S. Wang, T. Sakurai, W. Wen, Y. Qi, Energy level alignment at interfaces in metal halide perovskite solar cells, Adv. Mater. Interfac. 5 (2018), 1800260.

[49] Z. Yang, J. Dou, M. Wang, Interface engineering in n-i-p metal halide perovskite solar cells, Sol. RRL 2 (2018), 1800177.

[50] J. Chen, N.G. Park, Causes and solutions of recombination in perovskite solar cells, Adv. Mater. 31 (2019), 1803019.

[51] C. Ran, J. Xu, W. Gao, C. Huang, S. Dou, Defects in metal triiodide perovskite materials towards high-performance solar cells: origin, impact, characterization, and engineering, Chem. Soc. Rev. 47 (2018) 4581–4610.

[52] H. Wang, A. Guerrero, A. Bou, A.M. Al-Mayouf, J. Bisquert, Kinetic and material properties of interfaces governing slow response and long timescale phenomena in perovskite solar cells, Energy Environ. Sci. 12 (2019) 2054–2079.

[53] L.K. Ono, S. Liu, Y. Qi, Reducing detrimental defects for high-performance metal halide perovskite solar cells, Angew. Chem. Int. Ed. 59 (2020) 6676–6698.

[54] E. Mosconi, J.M. Azpiroz, F. Angelis, Ab initio molecular dynamics simulations of methylammonium lead iodide perovskite degradation by water, Chem. Mater. 27 (2015) 4885–4892.

[55] B. Wu, H.T. Nguyen, Z. Ku, G. Han, D. Giovanni, N. Mathews, H.J. Fan, T.C. Sum, Discerning the surface and bulk recombination kinetics of organic-inorganic halide perovskite single crystals, Adv. Energy Mater. 6 (2016), 1600551.

[56] Z. Ni, C. Bao, Y. Liu, Q. Jiang, W.-Q. Wu, S. Chen, X. Dai, B. Chen, B. Hartweg, Z. Yu, Z. Holman, J. Huang, Resolving spatial and energetic distributions of trap states in metal halide perovskite solar cells, Science 367 (2020) 1352–1358.

[57] D. Meggiolaro, E. Mosconi, F. Angelis, Modeling the interaction of molecular iodine with $MAPbI_3$: a probe of lead-halide perovskites defect chemistry, ACS Energy Lett. 3 (2018) 447–451.

[58] A. Rajagopal, K. Yao, A.K.Y. Jen, Toward perovskite solar cell commercialization: a perspective and research roadmap based on interfacial engineering, Adv. Mater. 30 (2018), 1800455.

[59] J. Berry, T. Buonassisi, D.A. Egger, G. Hodes, L. Kronik, Y.-L. Loo, I. Lubomirsky, S.R. Marder, Y. Mastai, J.S. Miller, D.B. Mitzi, Y. Paz, A.M. Rappe, I. Riess, B. Rybtchinski, O. Stafsudd, V. Stevanovic, M.F. Toney, D. Zitoun, A. Kahn, D. Ginley, D. Cahen, Hybrid organic-inorganic perovskites (HOIPs): opportunities and challenges, Adv. Mater. 27 (2015) 5102–5112.

[60] J. Chen, Y. Sheng, S. Ko, L. Liu, H. Han, X. Li, Push-pull porphyrins with different anchoring group orientations for fully printable monolithic dye-sensitized solar cells with mesoscopic carbon counter electrodes, New J. Chem. 39 (2015) 5231–5239.

[61] T. Handa, D.M. Tex, A. Shimazaki, A. Wakamiya, Y. Kanemitsu, Charge injection mechanism at heterointerfaces in $CH_3NH_3PbI_3$ perovskite solar cells revealed by simultaneous time-resolved photoluminescence and photocurrent measurements, J. Phys. Chem. Lett. 8 (2017) 954–960.

[62] V. D'Innocenzo, A.R.S. Kandada, M. Bastiani, M. Gandini, A. Petrozza, Tuning the light emission properties by band gap engineering in hybrid lead halide perovskite, J. Am. Chem. Soc. 136 (2014) 17730–17733.

[63] P. Singh, N.M. Ravindra, Temperature dependence of solar cell performance-an analysis, Sol. Energy Mater. Sol. Cells 101 (2012) 36–45.

[64] I.M. Los Santos, H.J. Cortina-Marrero, M.A. Ruíz-Sánchez, L. Hechavarría-Difur, F.J. Sánchez-Rodríguez, Ma Courel, H. Hu, Optimization of $CH_3NH_3PbI_3$ perovskite solar cells: a theoretical and experimental study, Sol. Energy 199 (2020) 198–205.

[65] H.J. Snaith, A. Abate, J.M. Ball, G.E. Eperon, T. Leijtens, N.K. Noel, S.D. Stranks, J.T.-W. Wang, K. Wojciechowski, W. Zhang, Anomalous hysteresis in perovskite solar cells, J. Phys. Chem. Lett. 5 (2014) 1511–1515.

[66] M.M. Tavakoli, D. Bi, L. Pan, A. Hagfeldt, S.M. Zakeeruddin, M. Grätzel, Adamantanes enhance the photovoltaic performance and operational stability of perovskite solar cells by effective mitigation of interfacial defect states, Adv. Energy Mater. 8 (2018), 1800275.

[67] N. Ahn, K. Kwak, M.S. Jang, H. Yoon, B.Y. Lee, J.-K. Lee, P.V. Pikhitsa, J. Byun, M. Choi, Trapped charge-driven degradation of perovskite solar cells, Nat. Commun. 7 (2016) 1–9.

[68] J. Wu, J. Shi, Y. Li, H. Li, H. Wu, Y. Luo, D. Li, Q. Meng, Quantifying the interface defect for the stability origin of perovskite solar cells, Adv. Energy Mater. 9 (2019), 1901352.

[69] S.H. Cho, J. Byeon, K. Jeong, J. Hwang, H. Lee, J. Jang, J. Lee, T. Kim, K. Kim, M. Choi, Y.S. Lee, Investigation of defect-tolerant perovskite solar cells with long-term stability via controlling the self-doping effect, Adv. Energy Mater. 11 (2021), 2100555.

[70] S. Lee, J.H. Park, B.R. Lee, E.D. Jung, J.C. Yu, D.D. Nuzzo, R.H. Friend, M.H. Song, Amine-based passivating materials for enhanced optical properties and performance of organic-inorganic perovskites in light-emitting diodes, J. Phys. Chem. Lett. 8 (2017) 1784–1792.

[71] Y.-S. Park, S. Guo, N.S. Makarov, V.I. Klimov, Room temperature single-photon emission from individual perovskite quantum dots, ACS Nano 9 (2015) 10386–10393.

[72] A. Swarnkar, R. Chulliyil, V.K. Ravi, M. Irfanullah, A. Chowdhury, A. Nag, Colloidal $CsPbBr_3$ perovskite nanocrystals: luminescence beyond traditional quantum dots, Angew. Chem., Int. Ed. 127 (2015) 15644–15648.

[73] F. Hu, H. Zhang, C. Sun, C. Yin, B. Lv, C. Zhang, W.W. Yu, X. Wang, Y. Zhang, M. Xiao, Superior optical properties of perovskite nanocrystals as single photon emitters, ACS Nano 9 (2015) 12410–12416.

[74] Y. Tian, A. Merdasa, M. Peter, M. Abdellah, K. Zheng, C.S. Ponseca Jr., T. Pullerits, A. Yartsev, V. Sundström, I.G. Scheblykin, Giant photoluminescence blinking of perovskite nanocrystals reveals single-trap control of luminescence, Nano Lett. 15 (2015) 1603–1608.

[75] I.Y. Eremchev, A.O. Tarasevich, J. Li, A.V. Naumov, I.G. Scheblykin, Lack of photon antibunching supports supertrap model of photoluminescence blinking in perovskite sub-micrometer crystals, Adv. Opt. Mater. 9 (2021), 2001596.

[76] K. Saxena, V. Jain, D.S. Mehta, A review on the light extraction techniques in organic electroluminescent devices, Opt. Mater. 32 (2009) 221–233.

[77] I.D. Parker, Carrier tunneling and device characteristics in polymer light-emitting diodes, J. Appl. Phys. 75 (1994) 1656–1666.

[78] Y. Ke, N. Wang, D. Kong, Y. Cao, Y. He, L. Zhu, Y. Wang, C. Xue, Q. Peng, F. Gao, W. Huang, J. Wang, Defect passivation for red perovskite light-emitting diodes with improved brightness and stability, J. Phys. Chem. Lett. 10 (2019) 380–385.

[79] S. Hou, M.K. Gangishetty, Q. Quan, D.N. Congreve, Efficient blue and white perovskite light-emitting diodes via manganese doping, Joule 2 (2018) 2421–2433.

[80] W. Xu, Q. Hu, S. Bai, C. Bao, Y. Miao, Z. Yuan, T. Borzda, A.J. Barker, E. Tyukalova, Z. Hu, M. Kawecki, H. Wang, Z. Yan, X. Liu, X. Shi, K. Uvdal, M. Fahlman, W. Zhang, M. Duchamp, J.-M. Liu, A. Petrozza, J. Wang, L.-M. Liu, W. Huang, F. Gao, Rational molecular passivation for high-performance perovskite light-emitting diodes, Nat. Photonics 13 (2019) 418–424.

[81] H. Li, H. Lin, D. Ouyang, C. Yao, C. Li, J. Sun, Y. Song, Y. Wang, Y. Yan, Y. Wang, Q. Dong, W.C.H. Choy, Efficient and stable red perovskite light-emitting diodes with operational stability >300 h, Adv. Mater. 33 (2021), 2008820.

[82] F. Winterer, L.S. Walter, J. Lenz, S. Seebauer, Y. Tong, L. Polavarapu, R.T. Weitz, Charge traps in all-inorganic $CsPbBr_3$ perovskite nanowire field-effect phototransistors, Adv. Electron. Mater. 7 (2021), 2100105.

[83] M.S. Fuhrer, J. Hone, Measurement of mobility in dual-gated MoS_2 transistors, Nat. Nanotechnol. 8 (2013) 146–147.

[84] J. Zaumseil, H. Sirringhaus, Electron and ambipolar transport in organic field-effect transistors, Chem. Rev. 107 (2007) 1296–1323.

[85] C. Eames, J.M. Frost, P.R.F. Barnes, B.C. O'Regan, A. Walsh, M.S. Islam, Ionic transport in hybrid lead iodide perovskite solar cells, Nat. Commun. 6 (2015) 1–8.

[86] S. Meloni, T. Moehl, W. Tress, M. Franckevičius, M. Saliba, Y.H. Lee, P. Gao, M.K. Nazeeruddin, S.M. Zakeeruddin, U. Rothlisberger, M. Graetzel, Ionic polarization-induced current-voltage hysteresis in $CH_3NH_3PbX_3$ perovskite solar cells, Nat. Commun. 7 (2016) 1–9.

[87] S.P. Senanayak, B. Yang, T.H. Thomas, N. Giesbrecht, W. Huang, E. Gann, B. Nair, K. Goedel, S. Guha, X. Moya, C.R. Mcneill, P. Docampo, A. Sadhanala, R. H. Friend, H. Sirringhaus, Understanding charge transport in lead iodide perovskite thin-film field-effect transistors, Sci. Adv. 3 (2017), e1601935.

[88] D. Li, H.-C. Cheng, Y. Wang, Z. Zhao, G. Wang, H. Wu, Q. He, Y. Huang, X. Duan, The effect of thermal annealing on charge transport in organolead halide perovskite microplate field-effect transistors, Adv. Mater. 29 (2017), 1601959.

[89] L. Lei, Q. Dong, K. Gundogdu, F. So, Metal halide perovskites for laser applications, Adv. Funct. Mater. 31 (2021), 2010144.

[90] L.M. Herz, Charge-carrier dynamics in organic-inorganic metal halide perovskites, Annu. Rev. Phys. Chem. 67 (2016) 65–89.

[91] Y. Yamada, T. Nakamura, M. Endo, A. Wakamiya, Y. Kanemitsu, Photocarrier recombination dynamics in perovskite $CH_3NH_3PbI_3$ for solar cell applications, J. Am. Chem. Soc. 136 (2014) 11610–11613.

[92] G. Xing, N. Mathews, S.S. Lim, N. Yantara, X. Liu, D. Sabba, M. Grätzel, S. Mhaisalkar, T.C. Sum, Low-temperature solution-processed wavelength-tunable perovskites for lasing, Nat. Mater. 13 (2014) 476–480.

[93] G. Xing, B. Wu, X. Wu, M. Li, B. Du, Q. Wei, J. Guo, E.K.L. Yeow, T.C. Sum, W. Huang, Transcending the slow bimolecular recombination in lead-halide perovskites for electroluminescence, Nat. Commun. 8 (2017) 1–9.

[94] A. Buin, P. Pietsch, J. Xu, O. Voznyy, A.H. Ip, R. Comin, E.H. Sargent, Materials processing routes to trap-free halide perovskites, Nano Lett. 14 (2014) 6281–6286.

[95] G. Xing, N. Mathews, S. Sun, S.S. Lim, T.M. Lam, M. Grätzel, S. Mhaisalkar, T.C. Sum, Long-range balanced electron-and hole-transport lengths in organic-inorganic $CH_3NH_3PbI_3$, Science 342 (2013) 344–347.

[96] D. Yan, T. Shi, Z. Zang, S. Zhao, J. Du, Y. Leng, Stable and low-threshold whispering-gallery-mode lasing from modified $CsPbBr_3$ perovskite quantum dots@ SiO_2 sphere, Chem. Eng. J. 401 (2020), 126066.

[97] M. Li, Q. Shang, C. Li, S. Li, Y. Liang, W. Yu, C. Wu, L. Zhao, Y. Zhong, W. Du, X. Wu, Z. Jia, Y. Gao, H. Chen, X. Liu, S. Guo, Q. Liao, G. Xing, L. Xiao, Q. Zhang, High optical gain of solution-processed mixed-cation $CsPbBr_3$ thin films towards enhanced amplified spontaneous emission, Adv. Funct. Mater. 31 (2021), 2102210.

[98] D.F. Swinehart, The beer-lambert law, J. Chem. Educ. 39 (1962) 333–335.

[99] Y. Zhao, H. Tan, H. Yuan, Z. Yang, J.Z. Fan, J. Kim, O. Voznyy, X. Gong, L.N. Quan, C.S. Tan, J. Hofkens, D. Yu, Q. Zhao, E.H. Sargent, Perovskite seeding growth of formamidinium-lead-iodide-based perovskites for efficient and stable solar cells, Nat. Commun. 9 (2018) 1607.

[100] G. Yang, Z. Ni, Z.J. Yu, B.W. Larson, Z. Yu, B. Chen, A. Alasfour, X. Xiao, J.M. Luther, Z.C. Holman, J. Huang, Defect engineering in wide-bandgap perovskites for efficient perovskite–silicon tandem solar cells, Nat. Photonics 16 (2022) 588–594.

[101] S. Singh, Laxmi, D. Kabra, Defects in halide perovskite semiconductors: impact on photo-physics and solar cell performance, J. Phys. D Appl. Phys. 53 (2020), 503003.
[102] R. Wang, J. Xue, L. Meng, J.-W. Lee, Z. Zhao, P. Sun, L. Cai, T. Huang, Z. Wang, Z.-K. Wang, Y. Duan, J.L. Yang, S. Tan, Y. Yuan, Y. Huang, Y. Yang, Caffeine improves the performance and thermal stability of perovskite solar cells, Joule 3 (2019) 1464–1477.
[103] G.Y. Kim, S.H. Oh, B.P. Nguyen, W. Jo, B.J. Kim, D.G. Lee, H.S. Jung, Efficient carrier separation and intriguing switching of bound charges in inorganic-organic lead halide solar cells, J. Phys. Chem. Lett. 6 (2015) 2355–2362.
[104] N. Li, S. Tao, Y. Chen, X. Niu, C.K. Onwudinanti, C. Hu, Z. Qiu, Z. Xu, G. Zheng, L. Wang, Y. Zhang, L. Li, H. Liu, Y. Lun, J. Hong, X. Wang, Y. Liu, H. Xie, Y. Gao, Y. Bai, S. Yang, G. Brocks, Q. Chen, H. Zhou, Cation and anion immobilization through chemical bonding enhancement with fluorides for stable halide perovskite solar cells, Nat. Energy 4 (2019) 408–415.
[105] W. Ke, C. Xiao, C. Wang, B. Saparov, H.-S. Duan, D. Zhao, Z. Xiao, P. Schulz, S.P. Harvey, W. Liao, W. Meng, Y. Yu, A.J. Cimaroli, C.-S. Jiang, K. Zhu, M. Al-Jassim, G. Fang, D.B. Mitzi, Y. Yan, Employing lead thiocyanate additive to reduce the hysteresis and boost the fill factor of planar perovskite solar cells, Adv. Mater. 28 (2016) 5214–5221.
[106] S. Bai, P. Da, C. Li, Z. Wang, Z. Yuan, F. Fu, M. Kawecki, X. Liu, N. Sakai, J.T.-W. Wang, S. Huettner, S. Buecheler, M. Fahlman, F. Gao, H.J. Snaith, Planar perovskite solar cells with long-term stability using ionic liquid additives, Nature 571 (2019) 245–250.
[107] G. Jin, T. Liu, Y. Li, J. Zhou, D. Zhang, P. Pang, Z. Ye, Z. Xing, G. Xing, J. Chen, D. Ma, Low-dimensional phase suppression and defect passivation of quasi-2D perovskites for efficient electroluminescence and low-threshold amplified spontaneous emission, Nanoscale 14 (2022) 919–929.
[108] Q. Jiang, L. Zhang, H. Wang, X. Yang, J. Meng, H. Liu, Z. Yin, J. Wu, X. Zhang, J. You, Enhanced electron extraction using SnO_2 for high-efficiency planar-structure $HC(NH_2)_2PbI_3$-based perovskite solar cells, Nat. Energy 2 (2016) 1–7.
[109] D.-Y. Son, S.-G. Kim, J.-Y. Seo, S.-H. Lee, H. Shin, D. Lee, N.-G. Park, Universal approach toward hysteresis-free perovskite solar cell via defect engineering, J. Am. Chem. Soc. 140 (2018) 1358–1364.
[110] X. Gong, L. Guan, H. Pan, Q. Sun, X. Zhao, H. Li, H. Pan, Y. Shen, Y. Shao, L. Sun, Z. Cui, L. Ding, M. Wang, Highly efficient perovskite solar cells via nickel passivation, Adv. Funct. Mater. 28 (2018), 1804286.
[111] D. Cortecchia, W. Mróz, S. Neutzner, T. Borzda, G. Folpini, R. Brescia, A. Petrozza, Defect engineering in 2D perovskite by Mn (II) doping for light-emitting applications, Chem 5 (2019) 2146–2158.
[112] I. Spanopoulos, I. Hadar, W. Ke, P. Guo, E.M. Mozur, E. Morgan, S. Wang, D. Zheng, S. Padgaonkar, G.N.M. Reddy, E.A. Weiss, M.C. Hersam, R. Seshadri, R. D. Schaller, M.G. Kanatzidis, Tunable broad light emission from 3D "hollow" bromide perovskites through defect engineering, J. Am. Chem. Soc. 143 (2021) 7069–7080.
[113] D. Ghosh, A.R. Smith, A.B. Walker, M.S. Islam, Mixed A-cation perovskites for solar cells: atomic-scale insights into structural distortion, hydrogen bonding, and electronic properties, Chem. Mater. 30 (2018) 5194–5204.
[114] D.W. Ferdani, S.R. Pering, D. Ghosh, P. Kubiak, A.B. Walker, S.E. Lewis, A.L. Johnson, P.J. Baker, M.S. Islam, P.J. Cameron, Partial cation substitution reduces iodide ion transport in lead iodide perovskite solar cells, Energy Environ. Sci. 12 (2019) 2264–2272.
[115] S.P. Senanayak, M. Abdi-Jalebi, V.S. Kamboj, R. Carey, T. Tian, G. Schweicher, J. Wang, N. Giesbrecht, D.D. Nuzzo, H.E. Beere, P. Docampo, D.A. Ritchie, D. Fairen-Jimenez, R.H. Friend, H. Sirringhaus, A general approach for hysteresis-free, operationally stable metal halide perovskite field-effect transistors, Sci. Adv. 6 (2020), eaaz4948.
[116] C. Bi, S. Wang, Q. Li, S.V. Kershaw, J. Tian, A.L. Rogach, Thermally stable copper(II)-doped cesium lead halide perovskite quantum dots with strong blue emission, J. Phys. Chem. Lett. 10 (2019) 943–952.
[117] Z.-J. Yong, S.-Q. Guo, J.-P. Ma, J.-Y. Zhang, Z.-Y. Li, Y.-M. Chen, B.-B. Zhang, Y. Zhou, J. Shu, J.-L. Gu, L.-R. Zheng, O.M. Bakr, H.-T. Sun, Doping-enhanced short-range order of perovskite nanocrystals for near-unity violet luminescence quantum yield, J. Am. Chem. Soc. 140 (2018) 9942–9951.
[118] J. Yin, G.H. Ahmed, O.M. Bakr, J.L. Brédas, O.F. Mohammed, Unlocking the effect of trivalent metal doping in all-inorganic $CsPbBr_3$ perovskite, ACS Energy Lett. 4 (2019) 789–795.
[119] J.-S. Yao, J. Ge, B.-N. Han, K.-H. Wang, H.-B. Yao, H.-L. Yu, J.-H. Li, B.-S. Zhu, J.-Z. Song, C. Chen, Q. Zhang, H.-B. Zeng, Y. Luo, S.-H. Yu, Ce^{3+}-doping to modulate photoluminescence kinetics for efficient $CsPbBr_3$ nanocrystals based light-emitting diodes, J. Am. Chem. Soc. 140 (2018) 3626–3634.
[120] Y.J. Lee, J.S. Han, D.E. Lee, T.H. Lee, J.Y. Kim, J.M. Suh, J.H. Lee, I.H. Im, S.J. Kim, K.J. Kwak, H.W. Jang, in: High Hole Mobility Inorganic Halide Perovskite Field-Effect Transistors with Enhanced Phase Stability and Interfacial Defect Tolerance, vol. 8, 2022, 2100624.
[121] A. Sadhanala, S. Ahmad, B. Zhao, N. Giesbrecht, P.M. Pearce, F. Deschler, R.L.Z. Hoye, K.C. Gödel, T. Bein, P. Docampo, S.E. Dutton, M.F.L. Volder, R. H. Friend, Blue-green color tunable solution processable organolead chloride-bromide mixed halide perovskites for optoelectronic applications, Nano Lett. 15 (2015) 6095–6101.
[122] T. Neumann, S. Feldmann, P. Moser, A. Delhomme, J. Zerhoch, T. Goor, S. Wang, M. Dyksik, T. Winkler, J.J. Finley, P. Plochocka, M.S. Brandt, C. Faugeras, A. V. Stier, F. Deschler, Manganese doping for enhanced magnetic brightening and circular polarization control of dark excitons in paramagnetic layered hybrid metal-halide perovskites, Nat. Commun. 12 (2021) 3489.
[123] L. Wang, C. McCleese, A. Kovalsky, Y. Zhao, C. Burda, Femtosecond time-resolved transient absorption spectroscopy of $CH_3NH_3PbI_3$ perovskite films: evidence for passivation effect of PbI_2, J. Am. Chem. Soc. 136 (2014) 12205–12208.
[124] Y.C. Kim, N.J. Jeon, J.H. Noh, W.S. Yang, J. Seo, J.S. Yun, A. Ho-Baillie, S. Huang, M.A. Green, J. Seidel, T.K. Ahn, S. II Seok, Beneficial effects of PbI_2 incorporated in organo-lead halide perovskite solar cells, Adv. Energy Mater. 6 (2016), 1502104.
[125] M.I.H. Ansaria, A. Qurashib, M.K. Nazeeruddin, Frontiers, opportunities, and challenges in perovskite solar cells: a critical review, J. Photochem. Photobiol. C Photochem. Rev. 35 (2018) 1–24.
[126] C. Roldán-Carmona, P. Gratia, I. Zimmermann, G. Grancini, P. Gao, M. Graetzel, M.K. Nazeeruddin, High efficiency methylammonium lead triiodide perovskite solar cells: the relevance of non-stoichiometric precursors, Energy Environ. Sci. 8 (2015) 3550–3556.
[127] Q. Chen, H. Zhou, T.-B. Song, S. Luo, Z. Hong, H.-S. Duan, L. Dou, Y. Liu, Y. Yang, Controllable self-induced passivation of hybrid lead iodide perovskites toward high performance solar cells, Nano Lett. 14 (2014) 4158–4163.
[128] Y. Chen, Q. Meng, Y. Xiao, X. Zhang, J. Sun, C.B. Han, H. Gao, Y. Zhang, Y. Lu, H. Yan, Mechanism of PbI_2 in situ passivated perovskite films for enhancing the performance of perovskite solar cells, ACS Appl. Mater. Interfaces 11 (2019) 44101–44108.
[129] C.-C. Zhang, M. Li, Z.-K. Wang, Y.-R. Jiang, H.-R. Liu, Y.-G. Yang, X.-Y. Gao, H. Ma, Passivated perovskite crystallization and stability in organic-inorganic halide solar cells by doping a donor polymer, J. Mater. Chem. 5 (2017) 2572–2579.
[130] L.A. Frolova, A.I. Davlethanov, N.N. Dremova, I. Zhidkov, A.F. Akbulatov, E.Z. Kurmaev, S.M. Aldoshin, K.J. Stevenson, P.A. Troshin, Efficient and stable $MAPbI_3$-based perovskite solar cells using polyvinylcarbazole passivation, J. Phys. Chem. Lett. 11 (2020) 6772–6778.
[131] X.-J. She, C. Chen, G. Divitini, B. Zhao, Y. Li, J. Wang, J.F. Orri, L. Cui, W. Xu, J. Peng, S. Wang, A. Sadhanala, Henning Sirringhaus, A solvent-based surface cleaning and passivation technique for suppressing ionic defects in high-mobility perovskite field-effect transistors, Nat. Electron. 3 (2020) 694–703.
[132] H.P. Kim, M. Vasilopoulou, H. Ullah, S. Bibi, A.E.X. Gavim, A.G. Macedo, W.J. da Silva, F.K. Schneider, A.A. Tahir, M.A.M. Teridi, P. Gao, A.R.M. Yusoff, M. K. Nazeeruddin, A hysteresis-free perovskite transistor with exceptional stability through molecular cross-linking and amine-based surface passivation, Nanoscale 12 (2020) 7641–7650.
[133] H.P. Kim, M. Vasilopoulou, H. Ullah, S. Bibi, A.E.X. Gavim, A.G. Macedo, W.J. da Silva, F.K. Schneider, A.A. Tahir, M.A.M. Teridi, P. Gao, A.R.M. Yusoff, M. K. Nazeeruddin, A hysteresis-free perovskite transistor with exceptional stability through molecular cross-linking and amine-based surface passivation, Nanoscale 12 (2020) 7641–7650.
[134] T. Webb, S.J. Sweeney, W. Zhang, Device architecture engineering: progress toward next generation perovskite solar cells, Adv. Funct. Mater. 31 (2021), 2103121.
[135] N.K. Noel, A. Abate, S.D. Stranks, E.S. Parrott, V.M. Burlakov, A. Goriely, H.J. Snaith, Enhanced photoluminescence and solar cell performance via Lewis base passivation of organic-inorganic lead halide perovskites, ACS Nano 8 (2014) 9815–9821.

[136] D.W. deQuilettes, S. Koch, S. Burke, R.K. Paranji, A.J. Shropshire, M.E. Ziffer, D.S. Ginger, Photoluminescence lifetimes exceeding 8 μs and quantum yields exceeding 30% in hybrid perovskite thin films by ligand passivation, ACS Energy Lett. 1 (2016) 438–444.
[137] L. Zhu, Y. Xu, P. Zhang, J. Shi, Y. Zhao, H. Zhang, J. Wu, Y. Luo, D. Li, Q. Meng, Investigation on the role of Lewis bases in the ripening process of perovskite films for highly efficient perovskite solar cells, J. Mater. Chem. 5 (2017) 20874–20881.
[138] R.J.E. Westbrook, T.J. Macdonald, W. Xu, L. Lanzetta, J.M. Marin-Beloqui, T.M. Clarke, S.A. Haque, Lewis base passivation mediates charge transfer at perovskite heterojunctions, J. Am. Chem. Soc. 143 (2021) 12230–12243.
[139] R. Yang, Y.-Q. Li, M.-L. Guo, X.-Y. Cai, J.-X. Tang, Efficient pure-red perovskite light-emitting diodes using dual-Lewis-base molecules for interfacial modification, J. Mater. Chem. C 9 (2021) 9169–9177.
[140] Y. Shao, Z. Xiao, C. Bi, Y. Yuan, J. Huang, Origin and elimination of photocurrent hysteresis by fullerene passivation in $CH_3NH_3PbI_3$ planar heterojunction solar cells, Nat. Commun. 5 (2014) 1–7.
[141] Y. Lin, L. Shen, J. Dai, Y. Deng, Y. Wu, Y. Bai, X. Zheng, J. Wang, Y. Fang, H. Wei, W. Ma, X.C. Zeng, X. Zhan, J. Huang, π-conjugated Lewis base: efficient trap-passivation and charge-extraction for hybrid perovskite solar cells, Adv. Mater. 29 (2017), 1604545.
[142] G. Yang, P. Qin, G. Fang, G. Li, A Lewis base-assisted passivation strategy towards highly efficient and stable perovskite solar cells, Sol. RRL 2 (2018), 1800055.
[143] J. Xu, A. Buin, A.H. Ip, W. Li, O. Voznyy, R. Comin, M. Yuan, S. Jeon, Z. Ning, J.J. McDowell, P. Kanjanaboos, J.-P. Sun, X. Lan, L.N. Quan, D.H. Kim, I.G. Hill, P. Maksymovych, E.H. Sargent, Perovskite-fullerene hybrid materials suppress hysteresis in planar diodes, Nat. Commun. 6 (2015) 1–8.
[144] C. Park, H. Ko, D.H. Sin, K.C. Song, K. Cho, Organometal halide perovskite solar cells with improved thermal stability via grain boundary passivation using a molecular additive, Adv. Funct. Mater. 27 (2017), 1703546.
[145] F. Cai, L. Yang, Y. Yan, J. Zhang, F. Qin, D. Liu, Y.-B. Cheng, Y. Zhou, Tao Wang, Eliminated hysteresis and stabilized power output over 20% in planar heterojunction perovskite solar cells by compositional and surface modifications to the low-temperature-processed TiO_2 layer, J. Mater. Chem. 5 (2017) 9402–9411.
[146] S. Song, S.J. Yang, J. Choi, S.G. Han, K. Park, H. Lee, J. Min, S. Ryu, K. Cho, Surface stabilization of a formamidinium perovskite solar cell using quaternary ammonium salt, ACS Appl. Mater. Interfaces 13 (2021) 37052–37062.
[147] D. Zheng, R. Peng, G. Wang, J.L. Logsdon, B. Wang, X. Hu, Y. Chen, V.P. Dravid, M.R. Wasielewski, J. Yu, W. Huang, Z. Ge, T.J. Marks, A. Facchetti, Simultaneous bottom-up interfacial and bulk defect passivation in highly efficient planar perovskite solar cells using nonconjugated small-molecule electrolytes, Adv. Mater. 31 (2019), 1903239.
[148] L. Zuo, H. Guo, D.W. deQuilettes, S. Jariwala, N. Marco, S. Dong, R. Deblock, D.S. Ginger, B. Dunn, M. Wang, Y. Yang, Polymer-modified halide perovskite films for efficient and stable planar heterojunction solar cells, Sci. Adv. 3 (2017), e1700106.
[149] S. Wang, Z. Ma, B. Liu, W. Wu, Y. Zhu, R. Ma, C. Wang, High-performance perovskite solar cells with large grain-size obtained by using the Lewis acid-base adduct of thiourea, Sol. RRL 2 (2018), 1800034.
[150] K. Sun, Z. Hu, B. Shen, C. Lu, L. Huang, J. Zhang, J. Zhang, Y. Zhu, Lewis acid-base interaction-induced porous PbI_2 film for efficient planar perovskite solar cells, ACS Appl. Energy Mater. 1 (2018) 2114–2122.
[151] I. Nakamura, N. Negishi, S. Kutsuna, T. Ihara, S. Sugihara, K. Takeuchi, Role of oxygen vacancy in the plasma-treated TiO_2 photocatalyst with visible light activity for NO removal, J. Mol. Catal. Chem. 161 (2000) 205–212.
[152] J.M. Azpiroz, E. Mosconi, J. Bisquert, F. Angelis, Defect migration in methylammonium lead iodide and its role in perovskite solar cell operation, Energy Environ. Sci. 8 (2015) 2118–2127.
[153] T. Leijtens, G.E. Eperon, S. Pathak, A. Abate, M.M. Lee, H.J. Snaith, Overcoming ultraviolet light instability of sensitized TiO_2 with meso-superstructured organometal tri-halide perovskite solar cells, Nat. Commun. 4 (2013) 1–8.
[154] Y. Ogomi, A. Morita, S. Tsukamoto, T. Saitho, Q. Shen, T. Toyoda, K. Yoshino, S.S. Pandey, T. Ma, Shuzi Hayase, All-solid perovskite solar cells with HOCO-R-NH^{3+} I-anchor-group inserted between porous titania and perovskite, J. Phys. Chem. C 118 (2014) 16651–16659.
[155] K. Wojciechowski, S.D. Stranks, A. Abate, G. Sadoughi, A. Sadhanala, N. Kopidakis, G. Rumbles, C.-Z. Li, R.H. Friend, A.K.-Y. Jen, H.J. Snaith, Heterojunction modification for highly efficient organic-inorganic perovskite solar cells, ACS Nano 8 (2014) 12701–12709.
[156] S.K. Pathak, A. Abate, P. Ruckdeschel, B. Roose, K.C. Gödel, Y. Vaynzof, A. Santhala, S.-I. Watanabe, D.J. Hollman, N. Noel, A. Sepe, U. Wiesner, R. Friend, H. J. Snaith, U. Steiner, Performance and stability enhancement of dye-sensitized and perovskite solar cells by Al doping of TiO_2, Adv. Funct. Mater. 24 (2014) 6046–6055.
[157] J. Cao, B. Wu, R. Chen, Y. Wu, Y. Hui, B.-W. Mao, N. Zheng, Efficient, hysteresis-free, and stable perovskite solar cells with ZnO as electron-transport layer: effect of surface passivation, Adv. Mater. 30 (2018), 1705596.
[158] W. Ke, G. Fang, Q. Liu, L. Xiong, P. Qin, H. Tao, J. Wang, H. Lei, B. Li, J. Wan, G. Yang, Y. Yan, Low-temperature solution-processed tin oxide as an alternative electron transporting layer for efficient perovskite solar cells, J. Am. Chem. Soc. 137 (2015) 6730–6733.
[159] L. Zhang, X. Yang, Q. Jiang, P. Wang, Z. Yin, X. Zhang, H. Tan, Y. Yang, M. Wei, B.R. Sutherland, E.H. Sargent, J. You, Ultra-bright and highly efficient inorganic based perovskite light-emitting diodes, Nat. Commun. 8 (2017) 1–8.
[160] M.-H. Park, S.-H. Jeong, H.-K. Seo, C. Wolf, Y.-H. Kim, H. Kim, J. Byun, J.S. Kim, H. Cho, T.-W. Lee, Unravelling additive-based nanocrystal pinning for high efficiency organic-inorganic halide perovskite light-emitting diodes, Nano Energy 42 (2017) 157–165.
[161] Z. Xiao, R.A. Kerner, L. Zhao, N.L. Tran, K.M. Lee, T.-W. Koh, G.D. Scholes, B.P. Rand, Efficient perovskite light-emitting diodes featuring nanometre-sized crystallites, Nat. Photonics 11 (2017) 108–115.
[162] Z.-K. Tan, R.S. Moghaddam, M.L. Lai, P. Docampo, R. Higler, F. Deschler, M. Price, A. Sadhanala, L.M. Pazos, D. Credgington, F. Hanusch, T. Bein, H.J. Snaith, R.H. Friend, Bright light-emitting diodes based on organometal halide perovskite, Nat. Nanotechnol. 9 (2014) 687–692.
[163] F. Cai, J. Cai, L. Yang, W. Li, R.S. Gurney, H. Yi, A. Iraqi, D. Liu, T. Wang, Molecular engineering of conjugated polymers for efficient hole transport and defect passivation in perovskite solar cells, Nano Energy 45 (2018) 28–36.
[164] F. Zhang, X. Yang, M. Cheng, W. Wang, L. Sun, Boosting the efficiency and the stability of low cost perovskite solar cells by using CuPc nanorods as hole transport material and carbon as counter electrode, Nano Energy 20 (2016) 108–116.
[165] K. Domanski, J.-P. Correa-Baena, N. Mine, M.K. Nazeeruddin, A. Abate, M. Saliba, W. Tress, A. Hagfeldt, M. Grätzel, Not all that glitters is gold: metal-migration-induced degradation in perovskite solar cells, ACS Nano 10 (2016) 6306–6314.
[166] H. Back, G. Kim, J. Kim, J. Kong, T.K. Kim, H. Kang, H. Kim, J. Lee, S. Lee, K. Lee, Achieving long-term stable perovskite solar cells via ion neutralization, Energy Environ. Sci. 9 (2016) 1258–1263.
[167] X. Li, S. Fu, W. Zhang, S. Ke, W. Song, J. Fang, Chemical anti-corrosion strategy for stable inverted perovskite solar cells, Sci. Adv. 6 (2020), eabd1580.
[168] S.D. Stranks, S.M. Wood, K. Wojciechowski, F. Deschler, M. Saliba, H. Khandelwal, J.B. Patel, S.J. Elston, L.M. Herz, M.B. Johnston, A.P.H.J. Schenning, M. G. Debije, M.K. Riede, S.M. Morris, H.J. Snaith, Enhanced amplified spontaneous emission in perovskites using a flexible cholesteric liquid crystal reflector, Nano Lett. 15 (2015) 4935–4941.
[169] I.C. Smith, E.T. Hoke, D. Solis-Ibarra, M.D. McGehee, H.I. Karunadasa, A layered hybrid perovskite solar-cell absorber with enhanced moisture stability, Angew. Chem. Int. Ed. 53 (2014) 11232–11235.
[170] G. Grancini, C. Roldán-Carmona, I. Zimmermann, E. Mosconi, X. Lee, D. Martineau, S. Narbey, F. Oswald, F. Angelis, M. Graetzel, M.K. Nazeeruddin, One-year stable perovskite solar cells by 2D/3D interface engineering, Nat. Commun. 8 (2017) 1–8.
[171] F. Zhang, B. Cai, J. Song, B. Han, B. Zhang, H. Zeng, Efficient blue perovskite light-emitting diodes boosted by 2D/3D energy cascade channels, Adv. Funct. Mater. 30 (2020), 2001732.
[172] R. Azmi, E. Ugur, A. Seirkan, F. Aljamaan, A.S. Subbiah, J. Liu, G.T. Harrison, M.I. Nugraha, M.K. Eswaran, M. Babics, Y. Chen, F. Xu, T.G. Allen, A.U. Rehman, C.-L. Wang, T.D. Anthopoulos, U. Schwingenschlögl, M. Bastiani, E. Aydin, S. Wolf, Damp heat-stable perovskite solar cells with tailored-dimensionality 2D/3D heterojunctions, Science 376 (2022) 73–77.
[173] Z. Wang, Q. Lin, F.P. Chmiel, N. Sakai, L.M. Herz, H.J. Snaith, Efficient ambient-air-stable solar cells with 2D-3D heterostructured butylammonium-caesium-formamidinium lead halide perovskites, Nat. Energy 2 (2017), 17135.

[174] Y. Lin, Y. Bai, Y. Fang, Z. Chen, S. Yang, X. Zheng, S. Tang, Y. Liu, J. Zhao, J. Huang, Enhanced thermal stability in perovskite solar cells by assembling 2D/3D stacking structures, J. Phys. Chem. Lett. 9 (2018) 654–658.
[175] M.-G. La-Placa, L. Gil-Escrig, D. Guo, F. Palazon, T.J. Savenije, M. Sessolo, H.J. Bolink, Vacuum-deposited 2D/3D perovskite heterojunctions, ACS Energy Lett. 4 (2019) 2893–2901.
[176] Y. Tian, A. Merdasa, E. Unger, M. Abdellah, K. Zheng, S. McKibbin, A. Mikkelsen, T. Pullerits, A. Yartsev, V. Sundström, I.G. Scheblykin, Enhanced organo-metal halide perovskite photoluminescence from nanosized defect-free crystallites and emitting sites, J. Phys. Chem. Lett. 6 (2015) 4171–4177.
[177] H.-H. Fang, F. Wang, S. Adjokatse, N. Zhao, M.A. Loi, Photoluminescence enhancement in formamidinium lead iodide thin films, Adv. Funct. Mater. 26 (2016) 4653–4659.
[178] D.W. deQuilettes, W. Zhang, V.M. Burlakov, D.J. Graham, T. Leijtens, A. Osherov, V. Bulović, H.J. Snaith, D.S. Ginger, S.D. Stranks, Photo-induced halide redistribution in organic-inorganic perovskite films, Nat. Commun. 7 (2016) 1–9.
[179] E. Mosconi, D. Meggiolaro, H.J. Snaith, S.D. Stranks, F. Angelis, Light-induced annihilation of Frenkel defects in organo-lead halide perovskites, Energy Environ. Sci. 9 (2016) 3180–3187.
[180] H. Tsai, R. Asadpour, J.-C. Blancon, C.C. Stoumpos, O. Durand, J.W. Strzalka, B. Chen, R. Verduzco, P.M. Ajayan, S. Tretiak, J. Even, M.A. Alam, M. G. Kanatzidis, W. Nie, A.D. Mohite, Light-induced lattice expansion leads to high-efficiency perovskite solar cells, Science 360 (2018) 67–70.
[181] F.A. Roghabadi, N.M.R. Fumani, M. Alidaei, V. Ahmadi, S.M. Sadrameli, High power UV-light irradiation as a new method for defect passivation in degraded perovskite solar cells to recover and enhance the performance, Sci. Rep. 9 (2019) 1–11.
[182] X. Zhang, Z. Guo, R. Li, J. Yu, B. Zhen, B. Chen, T. He, R. Chen, Quasi-type II core-shell perovskite nanocrystals for improved structural stability and optical gain, ACS Appl. Mater. Interfaces 13 (2021) 58170–58178.
[183] Y. Shi, R. Li, G. Yin, X. Zhang, X. Yu, B. Meng, Z. Wei, R. Chen, Laser-induced secondary crystallization of $CsPbBr_3$ perovskite thin film for robust and low threshold amplified spontaneous emission, Adv. Funct. Mater. DOI: 10.1002/adfm.202207206..
[184] Z. Andaji-Garmaroudi, M. Anaya, A.J. Pearson, S.D. Stranks, Photobrightening in lead halide perovskites: observations, mechanisms, and future potential, Adv. Energy Mater. 10 (2021), 1903109.
[185] Q. Cao, S. Yang, Q. Gao, L. Lei, Y. Yu, J. Shao, Y. Liu, Fast and controllable crystallization of perovskite films by microwave irradiation process, ACS Appl. Mater. Interfaces 8 (2016) 7854–7861.
[186] Q. Chen, T. Ma, F. Wang, Y. Liu, S. Liu, J. Wang, Z. Cheng, Q. Chang, R. Yang, W. Huang, L. Wang, T. Qin, W. Huang, Rapid microwave-annealing process of hybrid perovskites to eliminate miscellaneous phase for high performance photovoltaics, Adv. Sci. 7 (2020), 2000480.
[187] Y. Wang, T. Chen, C. Huang, Y. Wang, J. Wu, B. Sun, Electrochemically switchable electrochemiluminescent sensor constructed based on inorganic perovskite quantum dots synthesized with microwave irradiation, J. Electroanal. Chem. 867 (2020), 114181.
[188] Z. Xu, Y. Jiang, Z. Li, C. Chen, X. Kong, Y. Chen, G. Zhou, J.-M. Liu, K. Kempa, J. Gao, Rapid microwave-assisted synthesis of SnO_2 quantum dots for efficient planar perovskite solar cells, ACS Appl. Energy Mater. 4 (2021) 1887–1893.
[189] R.J. Stewart, C. Grieco, A.V. Larsen, G.S. Doucette, J.B. Asbury, Molecular origins of defects in organohalide perovskites and their influence on charge carrier dynamics, J. Phys. Chem. C 120 (2016) 12392–12402.
[190] X. Li, D. Bi, C. Yi, J.-D. Décopprt, J. Luo, S.M. Zakeeruddin, A. Hagfeldt, M. Grätzel, A vacuum flash-assisted solution process for high-efficiency large-area perovskite solar cells, Science 353 (2016) 58–62.
[191] B.R. Sutherland, S. Hoogland, M.M. Adachi, P. Kanjanaboos, C.T.O. Wong, J.J. McDowell, J. Xu, O. Voznyy, Z. Ning, A.J. Houtepen, E.H. Sargent, Perovskite thin films via atomic layer deposition, Adv. Mater. 27 (2015) 53–58.
[192] W. Nie, H. Tsai, R. Asadpour, J.-C. Blancon, A.J. Neukirch, G. Gupta, J.J. Crochet, M. Chhowalla, S. Tretiak, M.A. Alam, H.-L. Wang, A.D. Mohite, High-efficiency solution-processed perovskite solar cells with millimeter-scale grains, Science 347 (2015) 522–525.
[193] A. AlMamun, T.T. Ava, T.M. Abdel-Fattah, H.J. Jeong, M.S. Jeong, S. Han, H. Yoon, G. Namkoong, Effect of hot-casted NiO hole transport layer on the performance of perovskite solar cells, Sol Energy188 (2019) 609–618.
[194] L. Dai, Z. Deng, F. Auras, H. Goodwin, Z. Zhang, J.C. Walmsley, P.D. Bristowe, F. Deschler, N.C. Greenham, Slow carrier relaxation in tin-based perovskite nanocrystals, Nat. Photonics 15 (2021) 696–702.
[195] Y. Chen, J. Yin, Q. Wei, C. Wang, X. Wang, H. Ren, S.F. Yu, O.M. Bakr, O.F. Mohammed, M. Li, Multiple exciton generation in tin-lead halide perovskite nanocrystals for photocurrent quantum efficiency enhancement, Nat. Photonics 16 (2022) 485–490.